

表 題 横紋筋融解症による急性腎障害における
AIM2 インフラマソームの役割

論 文 の 区 分 博士課程

著 者 名 バータルジャフ チントグトフ

担当指導教員氏名 高橋 将文 教授

所 属 自治医科大学大学院医学研究科
専攻 地域医療学系
専攻分野 血液・免疫疾患学
専攻科 炎症免疫学

2022 年 01 月 07 日申請の学位論文

Acknowledgements

I would like to sincerely thank my professor Masafumi Takahashi, for his vice guidance and support with full of encouragements. I am deeply thankful to my teacher Komada Takanori, for his immense knowledge and huge assistance. Their invaluable supports allow me to open new chapter of my life.

I greatly appreciate Tadayoshi Karasawa, Takayoshi Matsumura and Naoya Yamada for their critical advice and kind support.

This work would not have been possible without the support of those people. I would like to express my thanks to members of Division of Inflammation research, Naoko Sugaya, Rumiko Ochiai, Miyuki Hojo and Namiko Nakada.

It is my pleasure to thank to my teachers, Tsolmon Damdindorj who contributed great impact for my life. I would like to thank Choijamts Gotov, for being an amazing mentor.

It is my privilege to express my gratitude to precious people who always by my side. My heartfelt thanks to my dearest father Baatarjav Darikhoo and my lovely mother Sonin Nyamjav for everything you have given and done for us. Thank you for unconditional love and care. I am deeply grateful for my brothers and their families for always being with me.

Amarsanaa Lkhagvasuren, my better half, I cannot imagine myself without you. And my beautiful son Angarag Amarsanaa, I am the luckiest mom to have such an awesome son.

I am thankful to my friend, Ganbolor Jargalsaikhan for sharing and caring throughout my PhD.

Finally, I would like to thank to all my teachers, colleagues, relatives, and friends in great respects.

Abstract

Background: Rhabdomyolysis is a severe syndrome caused by muscle injury. During muscle lysis, components of muscle fiber, such as myoglobin, cytosolic contents, and DNA, can release into the bloodstream. The most common complication of rhabdomyolysis is acute kidney injury (AKI) which occasionally requires renal replacement therapy and influences patients' survival. Absent in melanoma 2 (AIM2), a cytosolic dsDNA sensor, leads to form an inflammasome. Inflammasome formation activates caspase-1 and secrete IL-1 β to enhance inflammation. However, AIM2 inflammasome-related mechanism is currently unknown in the pathophysiology of rhabdomyolysis-induced AKI (RIAKI).

Methods: To identify the role of AIM2 in rhabdomyolysis, we used WT, *Aim2*^{-/-} and ASC-citrine mice. For the rhabdomyolysis model, 5 ml/kg of 50% glycerol was intramuscularly injected on equally both hind limbs of 8-10 weeks old mice. Tissue samples were collected and evaluated by histological and immunohistological staining, RT-PCR, serum analysis, ELISA, flowcytometry, and western blotting.

Primary murine macrophages and kidney resident macrophages prepared from WT and *Aim2*^{-/-} were transfected by synthetic dsDNA, poly(dA:dT). Cell samples were evaluated by LDH assay, western blotting, live cell imaging, immunostaining, ELISA, and RT-PCR.

Results: We found DNase-I treatment improved tubular injury and inflammation after glycerol injection. That results suggested dsDNA can be a potential DAMP of RIAKI. Deletion of *Aim2* resulted in prolonged kidney injury and severe fibrosis after glycerol injection. We found M2 type of macrophages accumulated more in *Aim2*^{-/-} mice kidney and *Aim2*^{-/-} macrophages reduced pyroptosis and delayed elimination. Instead of rapid elimination by pyroptosis, *Aim2*^{-/-} macrophages activated STING to increase

inflammation.

M0/M2 polarized primary murine macrophages and kidney resident macrophages from WT induced pyroptosis without IL-1 β release after dsDNA treatment. On the other hand, *Aim2*^{-/-} macrophages were resistant to cell death and increased activity of cGAS/STING pathway in response to dsDNA.

Conclusions: We have demonstrated an unexpected role for AIM2-dependent pyroptosis in restricting inflammation. Our findings revealed that dsDNA/AIM2-dependent “homeostatic” pyroptosis in macrophages is essential for normal healing during RIAKI.

Contents

<i>List of the Figures</i>	3
<i>Abbreviations</i>	4
<i>Chapter 1. Introduction</i>	6
1-1. Rhabdomyolysis-induced acute kidney injury	6
1-2. DNA sensors	7
1-2.1. Absent in melanoma 2	7
1-2.2. cGAS/STING	10
1-2.3. AIM2 and other dsDNA sensors	10
1-3. Macrophages in RIAKI	11
<i>Chapter 2. Methods</i>	12
2-1. Mice and RIAKI model.	12
2-2. Cell culture	13
2-3. Real-time RT-PCR	14
2-4. Histology and immunostaining	16
2-4. Live cell imaging	17
2-5. Western blot	18
2-6. Flow cytometry	18
2-7. Serum chemistries	19
2-8. Picogreen assay	19

2-9. BrdU incorporation analysis	19
2-10. ELISA	20
2-11. Statistics	20
Chapter 3. Results	21
3-1. dsDNA was a potential DAMP during RIAKI.	21
3-2. <i>Aim2</i> ^{-/-} mice delayed recovery without disturbing tubular cells.	23
3-3. <i>Aim2</i> ^{-/-} exacerbated renal fibrosis after RIAKI.	27
3-4. Macrophages accumulated in <i>Aim2</i> ^{-/-} kidney during RIAKI.	29
3-5. Deletion of <i>Aim2</i> did not affect cell proliferation during RIAKI	33
3-6. Macrophage pyroptosis was restricted but NF- κ B was activated in <i>Aim2</i> ^{-/-} mice kidney during RIAKI.	34
3-7. dsDNA induced pyroptosis in distinct types of macrophages	38
3-8. STING signaling enhanced inflammation by dsDNA in the <i>Aim2</i> ^{-/-} -macrophages.	43
3-9. Survived macrophages from AIM2-pyroptosis enhanced the inflammation on surrounding cells.	46
Chapter 4. Discussion	47
Chapter 5. Conclusion	52
References	53

List of the Figures

Figure 1. AIM2 and cGAS/STING.....	9
Figure 2. DNase-I improved RIAKI	21
Figure 3. DNase-I ameliorated tubular injury and inflammation during RIAKI.....	22
Figure 4. Generation of <i>Aim2</i> ^{-/-} mice and genotyping	23
Figure 5. Confirmation phenotypes of <i>Aim2</i> ^{-/-} mice.	24
Figure 6. <i>Aim2</i> ^{-/-} did not affect muscle injury after glycerol injection.	25
Figure 7. <i>Aim2</i> ^{-/-} delayed recovery but tubular injury was similar.	26
Figure 8. <i>Aim2</i> ^{-/-} increased collagen accumulation after RIAKI.	27
Figure 9. <i>Aim2</i> ^{-/-} accelerated fibrosis after RIAKI.	28
Figure 10. Macrophages accumulated in <i>Aim2</i> ^{-/-} kidneys during RIAKI.....	29
Figure 11. M2 macrophages were dominant during RIAKI.	30
Figure 12. CXCR3 signaling contributed macrophage infiltration during RIAKI.	31
Figure 13. Neutrophils and lymphocytes played minor role during RIAKI.	32
Figure 14. Kidney BrdU incorporation analysis after glycerol injection.....	33
Figure 15. Flow cytometric analysis for cell death of macrophages in kidney.	34
Figure 16. Cell death of macrophages is less in <i>Aim2</i> ^{-/-} mice kidney.....	35
Figure 17. <i>Aim2</i> ^{-/-} restricted macrophage pyroptosis during RIAKI.	36
Figure 18. <i>Aim2</i> ^{-/-} enhanced NF-κB and TBK1 activation.	37
Figure 19. <i>Aim2</i> ^{-/-} macrophages resistant to dsDNA-induced pyroptosis.	39
Figure 20. Kidney resident macrophage isolation.	40
Figure 21. Kidney resident macrophages initiate dsDNA-induced pyroptosis without IL-1β release.	41
Figure 22. dsDNA induces pyroptosis in distinct types of macrophages.	42
Figure 23. <i>Aim2</i> ^{-/-} drive STING signaling by sensing dsDNA.	44
Figure 24. <i>Aim2</i> ^{-/-} macrophages produced inflammatory cytokines by STING.	45
Figure 25. Escape from AIM2-pyroptosis propagates inflammation to surrounding cells.	46
Figure 26. Graphical abstract.	51

Abbreviations

AIM2	Absent in melanoma 2
AKI	Acute kidney injury
ASC	Apoptosis-associated speck-like protein containing CARD
BMDM	Bone marrow-derived macrophages
BUN	Blood urea nitrogen
CHX	Cycloheximide
CKD	Chronic kidney disease
DAMP	Danger-associated molecular pattern
DNA	Deoxyribonucleic acid
EGF	Epithelial growth factor
FBS	Fetal bovine serum
cGAS	Cyclic GMP-AMP synthase
GSDMD	Gasdermin D
HRP	Horse radish peroxidase
IFN	Interferon
IHC	Immunohistochemistry
IRF3	Interferon regulatory transcription factor 3
KIM-1	Kidney injury molecule 1
KRM	Kidney resident macrophage
LDH	Lactate dehydrogenase
LPS	Lipopolysaccharide
NLRP3	NLR family pyrin domain containing 3

PAMP	Pathogen-associated molecular pattern
PAS	Periodic acid-Schiff
PBS	Phosphate-buffered saline
PRR	Pattern recognition receptor
RAAS	Renin angiotensin aldosterone system
RIAKI	Rhabdomyolysis-induced acute kidney injury
RNA	Ribonucleic acid
SDS	Sodium dodecyl sulphate
SMA	Smooth muscle actin
STING	Stimulator of interferon genes
TBK1	TANK binding kinase 1
TGF β	Transforming growth factor β
TLR9	Toll like receptor 9
TNF α	Tumor necrosis factor α
UUO	Unilateral ureteral obstruction

Chapter 1. Introduction

1-1. Rhabdomyolysis-induced acute kidney injury

Rhabdomyolysis is a syndrome characterized by damaged skeletal muscle releasing its cytosolic components into the bloodstream. As a result, muscle pain, elevated serum muscle cell enzymes such as creatine kinase (CK), and the presence of myoglobin in the urine (myoglobinuria) occur clinically¹⁻³.

The main causes of rhabdomyolysis are divided into 3 categories:

1. Trauma or muscle compression
 - o Car accident and natural disasters
 - o Prolonged restraint and immobilization
 - o Electrical injuries or burns.
2. Non-traumatic exertional
 - o Marathon runners
 - o Excessive physical training in humid heat conditions
 - o Untrained individuals
 - o Abnormal muscle metabolism disorders
3. Non-traumatic, non-exertional
 - o Drugs - central nervous system (CNS) depressants (heroin, cocaine, amphetamine), statins, colchicine, and dietary supplements
 - o Toxins - carbon dioxide, venoms, and fungal toxins
 - o Infections - influenza A and B, herpes simplex virus, HIV, Epstein Barr virus, SARS-CoV-2 (COVID -19) and others⁴

Symptoms can range from asymptomatic elevation of serum enzymes to life-threatening complications, including electrolyte disturbances, acute kidney injury (AKI), compartment

syndrome, and disseminated intravascular coagulation (DIC)⁵⁻⁷. AKI is reported in 5-30% of hospitalized patients with rhabdomyolysis^{6,8,9}. Patients with rhabdomyolysis-induced acute kidney injury (RIAKI) generally required renal replacement therapy, and 86-90% of these patients survived^{10,11}.

The pathogenesis of RIAKI is related to cytosolic components of the injured muscle such as myoglobin, which is thought to damage the kidney through tubular obstruction, formation of reactive oxygen species (ROS), and vasoconstriction. Also, the excessive leakage of extracellular fluid into the damaged muscle results in a loss of circulating volume and secondary activation of the renin-angiotensin-aldosterone system (RAAS). The activated RAAS constricts renal vessels and decreases renal blood flow, which exacerbates the pathological conditions of RIAKI¹².

dsDNA serves danger-associated molecular patterns (DAMPs), to be recognized by pattern recognition receptors (PRRs) and enhances inflammation. Self-derived dsDNA contributes to many diseases such as systemic lupus erythematosus, diabetes, cystic fibrosis, and cisplatin-induced AKI¹³⁻¹⁷. Although endogenous dsDNA (dsDNA) is also implicated in the pathogenesis of RIAKI¹⁸, its exact mechanism remains unclear.

1-2. DNA sensors

PRRs, essential components of innate immunity, recognize pathogen associated molecular patterns (PAMPs) or DAMPs and initiate an immune response. Among PRRs, many DNA-sensing receptors have been discovered: AIM2, cGAS/STING, TLR9, IFI16, DAI, DNA-PK, and DDX41.

1-2.1. Absent in melanoma 2 (AIM2)

AIM2, a cytosolic sensor for dsDNA, was first presented to have cancer-suppressive function in 1997¹⁹. In 2009, four groups independently discovered AIM2 as a dsDNA inflammasome-forming PRR²⁰⁻²³. AIM2 consists of a HIN200 domain at the C-terminus

and a PYD domain at the N-terminus. The HIN200 domain has the potential to bind only dsDNA, but not single-stranded DNA (ssDNA) or RNA. In response to dsDNA, AIM2 assembles an inflammasome with an adaptor protein (ASC) via its PYD domain and activates caspase-1 to produce the mature form of IL-1 β and the pore-forming protein N-terminal Gasdermin D (GSDMD). The mature IL-1 β is released into the extracellular space through the GSDMD pores at the cell membrane and water simultaneously enters the cell, leading to cell swelling and lysis. This GSDMD-dependent cell death is termed as pyroptosis (Fig. 1). The released mature IL-1 β triggers an inflammatory response to protect against viral or bacterial infection²⁴. For this reason, activation of the inflammasome is the effective self-defense mechanism in infectious diseases. Unfortunately, the formation of inflammasomes triggered by DAMPs increases inflammation and sometimes worsens the fate of the disease. Certain types of inflammasome-forming PRRs, including AIM2 and NLRP3, have been detected in both human and mouse kidneys²⁵. NLRP3 is a well-studied PRR associated with the pathogenesis of many AKI models by ischemia-reperfusion injury (IRI), folic acid, cisplatin, crystal, contrast agent, and rhabdomyolysis²⁶⁻³¹. In addition, NLRP3 in tubular cells has been shown to have an inflammasome-independent and aggravating effect during RIAKI. In the initial phase of RIAKI, ablation of NLRP3 attenuates renal inflammation and injury through decreasing lipid peroxidation, ferroptosis, and apoptosis in tubular cells³¹.

AIM2 is expressed in podocytes, tubular cells, and macrophages in the kidney³². A previous work has shown that AIM2 in macrophages plays an important role in the pathogenesis of chronic kidney disease (CKD). During unilateral ureteral obstruction (UUO), dsDNA from necrotic cells was taken up by macrophages, which activated the

AIM2 inflammasome and enhanced CKD³². However, the role of the AIM2 inflammasome in AKI is still unknown.

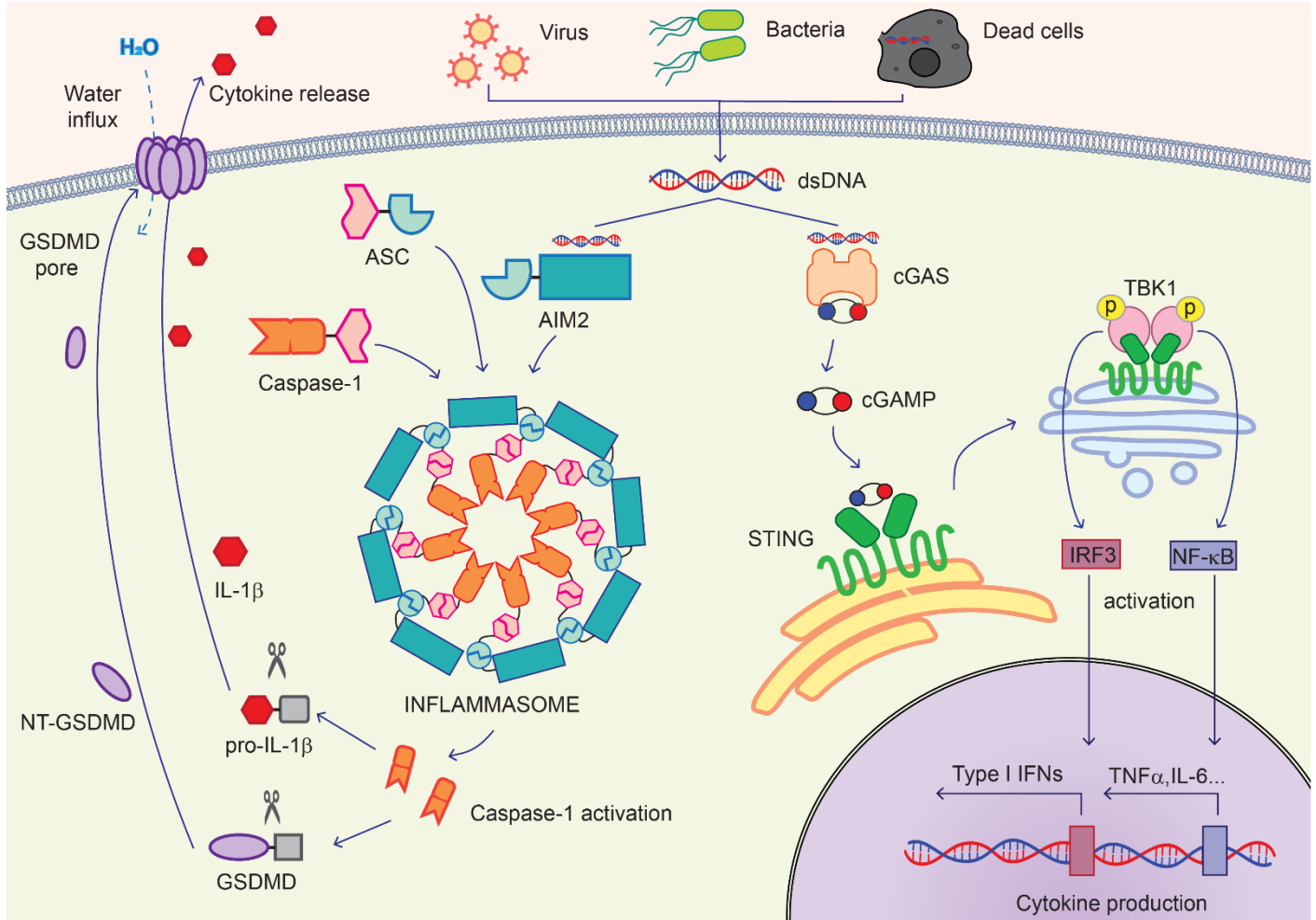


Figure 1. AIM2 and cGAS/STING.

dsDNA from pathogens and dead cells is recognized by the AIM2 and cGAS. HIN200 domain of AIM2 binds dsDNA and forms inflammasome with ASC and caspase 1. Inflammasome formation activates caspase 1 to cleaves pro-IL-1β to mature IL-1β and GSDMD to NT-GSDMD. NT-GSDMD makes pore on the cell membrane which serves cytokine efflux and water influx. Released cytokines such as IL-1β enhances inflammation and water influx results cell death. This inflammatory cell death is named “pyroptosis”.

After binds dsDNA, cGAS synthesizes cGAMP which is activator of STING. STING activation leads TBK1 recruitment to phosphorylate IRF3 and NF-κB. Phosphorylated IRF3 and NF-κB induces *de novo* cytokine production including type I IFNs, TNFα and IL-6.

1-2.2. cGAS/STING

The cyclic GMP-AMP synthase (cGAS) stimulator of interferon genes (STING) is a known dsDNA-sensing pathway that leads to activation of interferon regulatory factor 3 (IRF3) and NF- κ B to increase cytokine production. After cGAS recognizes dsDNA, cGAS synthesizes cyclic GMP-AMP (cGAMP), which binds to STING in the endoplasmic reticulum. Activated STING promotes autophosphorylation of TANK-binding kinase 1 (TBK1) and activation of NF- κ B. phosphorylated TBK1 phosphorylates IRF3 and enables dimerization and translocation of IRF3 into the nucleus to induce gene expression of type I interferons and other inflammatory cytokines (Fig. 1) ³³. cGAS/STING mediates not only signals of the defense mechanism against pathogens but also regulates cancer metabolism and autoimmunity^{33,34}. STING is expressed in many immune and non-immune cells and contributes to the pathogenesis of numerous non-infectious diseases such as systemic lupus erythematosus, nonalcoholic steatohepatitis, silicosis, traumatic brain injury, myocardial infarction, and renal diseases^{15,16,35-39}. Activation of STING by mitochondrial dsDNA in tubular cells contributes to the pathogenesis of AKI and renal fibrosis^{16,39}.

1-2.3. AIM2 and other dsDNA sensors

Several studies have suggested that deletion of AIM2 leads to activation of other dsDNA-sensing pathways such as cGAS/STING or DNA-dependent protein kinase (DNA-PK). The inhibitory effect of AIM2 on the cGAS/STING pathway has been explained as follows: caspase-1 activated by inflammasome formation directly cleaves cGAS⁴⁰ or K⁺ efflux through the GSDMD pores inhibits cGAS⁴¹.

Moreover, AIM2 directly forms a complex with DNA-PK and restricts the function of this enzyme^{42,43}. It should be noted that dsDNA sensors elicit broad innate immune responses.

However, how these sensors interact with each other or prioritize under specific conditions remains to be investigated.

1-3. Macrophages in RIAKI

Pyroptosis is an inflammatory form of cell death in macrophages because inflammasome activation occurs primarily in immune cells^{44,45}. Macrophages are considered to be a crucial regulator of AKI. Both macrophage subtypes, M1 and M2, contribute to the fate of AKI by regulating tubular regeneration, inflammatory reaction, or extracellular matrix deposition. To ensure normal healing after AKI, balance between M1 and M2 macrophages is necessary to be maintained for the microenvironment during the recovery phase of AKI. Indeed, M1/M2 macrophage imbalance, excessive accumulation, or ablation leads to inadequate healing⁴⁶⁻⁵⁰. However, how this balance during AKI is regulated has not been fully studied.

In the present study, we have demonstrated the AIM2-driven immunologically ‘silent’ pyroptosis, which may be beneficial for elimination of excessive macrophages in the later stage of RIAKI. Our study shows that dsDNA-AIM2 pyroptosis contributes to macrophage elimination and AIM2-deficiency alternatively activates cGAS/STING pathway, leading to the development of CKD.

Chapter 2. Methods

2-1. Mice and RIAKI model.

C57BL/6J wild-type mice (WT) were obtained from SLC Inc. (Shizuoka, Japan). *Aim2*^{-/-} mice on the C57BL/6J background were generated by CRISPR/Cas9-based genome editing at the Laboratory Animal Resource Centre, University of Tsukuba (Tsukuba, Japan). Genome editing in fertilized mouse eggs was performed using methods previously reported⁵¹. Exon 6 of the mouse *Aim2* allele WT (Genebank NC_000067.6) was selected for CRISPR/Cas9 deletion (Fig. 3A). *Aim2*^{-/-} mice developed normally and were genotyped with PCR primers 5'-TGGAGTTCAGGCAGATTCGG-3' and 5'-ATGTGGCACTCCGGTAGTATG-3' for a 310-bp product of WT DNA and 5'-TGGAGTTCAGGCAGATTCGG-3' and 5'-GTATGTGTGTTTGCCCACGC-3' for a 720-bp product of the mutant DNA (Fig. 3B). Inflammasome-activating phenotypes were validated using isolated mouse bone marrow-derived macrophages (mBMDMs) by treatment with lipopolysaccharide and poly(dA;dT) transfection (Fig. 4). *Asc*^{-/-}, *Casp1/11*^{-/-}, and *Gsdmd*^{-/-} mice were provided by Dr. Shun'ichiro Taniguchi (Shinshu University, Matsumoto, Japan), Hiroko Tsutsui (Hyogo University of Medicine, Nishinomiya, Japan), and Kate Schroder (The University of Queensland, Brisbane, Australia), respectively⁵²⁻⁵⁵. ASC citrine (B6.Cg-*Gt(ROSA)26Sor*^{tm1.1(CAG-Pycard/mCitrine*,CD2*)Dtg/J}) mice were obtained from The Jackson Laboratory (Bar Harbour, Maine, United States)⁵⁶. All mice were maintained on a 12-h light-dark cycle and received food and water ad libitum. Female mice aged 8-12 weeks were used for the cell experiments. Eight to 10 weeks old male mice were used for the RIAKI model. RIAKI was generated by intramuscular injection into both hind limbs with 50% glycerol (5 mL/kg) or vehicle (0.9% saline) after 24 hours of water deprivation⁵⁷. DNase-I (Sigma-Aldrich, St. Louis, MO, USA) was injected intraperitoneally (50KU) every 12 hours after the first 2 doses:

Immediately before (10KU) and after (50KU) glycerol injection. Control mice were injected with vehicle (PBS containing 0.15 mg/mL CaCl₂). Mice were sacrificed at the indicated time points after glycerol administration. All animal experiments were approved by Use and Care of Experimental Animals of Jichi Medical University Committee (#21021-01) and were performed according to the guidelines of Jichi Medical University.

2-2. Cell culture

Mouse bone marrow-derived macrophages (mBMDMs) were isolated from mouse femurs and tibias and cultured for 7 days in RPMI-1640 (Wako, Osaka, Japan) supplemented with 10% fetal bovine serum (FBS), 1% antibiotic antifungal solution (Sigma, St. Louis, MO, USA) and 15% conditioned medium of L929 cells (ATCC, Rockville, MD, USA) were added. mBMDMs were further cultured for 24 hours in the above medium containing 100 nM lipopolysaccharide (LPS, L4391, Sigma) and 10 ng/mL IFN γ (315-05, PeproTech, Cranbury, NJ, USA) for M(LPS/IFN γ) polarization. Media containing 20 ng/mL IL-4 (214-14, PeproTech), 10 ng/mL TGF β (100-21C, PeproTech) were used for 72-hour polarization of M(IL-4) and M(TGF β) respectively. To activate AIM2, cells were transfected with Poly(dA:dT) (InvivoGen, San Diego, CA, USA) using Lipofectamine 2000 (Thermo Fisher Scientific, Waltham, MA, USA) according to the manufacturer's protocol.

Primary tubular epithelial cells of the mouse kidney (mTECs) were isolated from mice as previously reported³². After sacrificing mice, the kidneys were immediately removed.

Kidney cortex was minced and incubated in RPMI 1640 containing 1 mg/mL collagenase D (11088866001, Sigma) at 37°C for one hour. Cells were passed through a 70- μ m cell strainer, washed twice with PBS (-) and plated on dishes. mTECs were grown in DMEM/F-12 medium containing 10% FBS, 125 ng/mL prostaglandin E1, 25 ng/mL EGF, 1.8 μ g/mL L-thyroxine, 3.38 ng/mL hydrocortisone and 2.5 mg/mL insulin-transferrin-

sodium selenite mix. Cells were grown at 37 °C in a 5% CO₂ atmosphere. Cells were used within 2 passages. For the AIM2 activation assay, cells were transfected with poly(dA:dT) using Lipofectamine 2000 and incubated for 24 hours.

Primary kidney resident macrophages (mKRM) were isolated from male WT and *Aim2*^{-/-} mice at 8-12 weeks of age. After perfusion with 10 mL saline from the heart, kidneys were harvested, minced, and digested for one hour at 37 °C in medium containing collagenase D (Sigma). After ACK buffer incubation for 8 minutes on ice, the cells were suspended in 40% Percoll (GE Healthcare) and a layer was formed on 80% Percoll followed by centrifugation at 500xg for 30 minutes without brake. Leukocytes at the interface were isolated, washed and resuspended in PBS. CD11b⁺ monocytes/macrophages were further purified using Mouse/Human CD11b MACS MicroBeads (130-049-601, Miltenyi Biotec, Bergisch Gladbach, Germany) according to the manufacturer's protocol. mKRM were grown for 2 days in RPMI-1640 containing 10 ng/mL M-CSF (315-02, PeproTech). J774 mouse macrophage-like cells were obtained from RIKEN gene bank (Tsukuba, Japan). Cells were cultured at 37 °C in a 5% CO₂ atmosphere and grown in RPMI-1640 supplemented with 10% FBS.

2-3. Real-time RT-PCR

Total RNA was isolated from whole kidney or cultured cells using ISOGEN (Nippon Gene, Toyama, Japan) according to the manufacturer's instructions. The primers used in our experiments are listed in following table.

Primer	Gene name	Primer sequence
<i>Actb</i>	Actin Beta	F: 5'-CACAGCTTCTTTGCAGCTCCTT-3' R: 5'-AGCGCAGCGATATCGTCAT-3'
<i>Arg1</i>	Arginase 1	F: 5'-ACAAGACAGGGCTCCTTTCA-3' R: 5'-AGCAAGCCAAGGTAAAGCC-3'
<i>Ccl2</i>	C-C Motif Chemokine Ligand 2	F: 5'-GGCTCAGCCAGATGCAGTTAAC-3' R: 5'-GCCTACTCATTGGGATCATCTTG-3'
<i>Ccr2</i>	C-C Motif Chemokine Receptor	F: 5'-CCTGCAAAGACCAGAAGAGGG-3' R: 5'-GAGATGTTGATAGTATGCCGTGGA-3'
<i>Ccr3</i>	C-C Motif Chemokine Receptor 3	F: 5'-TGGCAATTTCTGACCTGCTCT-3' R: 5'-AACCCAGACAGCATTTTGCAC-3'
<i>Ccr5</i>	C-C Motif Chemokine Receptor 5	F: 5'-CTGGCAAAAAGCTGAAGAGCGT-3' R: 5'-GCAGCATAGTGAGCCCAGAAT-3'
<i>Cd206</i>	Mannose Receptor C-Type 1	F: 5'-CAGGTGTGGGCTCAGGTAGT-3' R: 5'-TGTGGTGAGCTGAAAGGTGA-3'
<i>Cd68</i>	CD68 molecule	F: 5'-CTTCCCACAGGCAGCACAG-3' R: 5'-AATGATGAGAGGCAGCAAGAGG-3'
<i>Colla1</i>	Collagen Type I Alpha 1 Chain	F: 5'-GGGCGAGTGCTGTGCTTCCTG-3' R: 5'-CCTCGGTGTCCCTTCATTCCA-3'
<i>Cxcl10</i>	C-X-C Motif Chemokine Ligand 10	F: 5'-ACGTGTTGAGATCATTGCCA-3' R: 5'-GGCTCTCTGCTGTCCATCCAT-3'
<i>Cxcr3</i>	C-X-C Motif Chemokine Receptor 3	F: 5'-CGCAGCCCAAGTCCTAACACACT-3' R: 5'-CTGGCAGCAAAGTTACGGGTAAG-3'
<i>Foxp3</i>	Forkhead Box P3	F: 5'-CTCATGATAGTGCCTGTGTCCTCAA-3' R: 5'-AGGGCCAGCATAGGTGCAAG-3'
<i>Gapdh</i>	Glyceraldehyde-3-Phosphate Dehydrogenase	F: 5'-TGTGTCCGTCGTGGATCTGA-3' R: 5'-TTGCTGTTGAAGTCGCAGGAG-3'
<i>Havcr1</i> (KIM-1)	Hepatitis A Virus Cellular Receptor 1, Kidney Injury Molecule 1	F: 5'-CTGGAATGGCACTGTGACATCC-3' R: 5'-GCAGATGCCAACATAGAAGCCC-3'
<i>Ifnb1</i>	Interferon Beta 1	F: 5'-GCCTTTGCCATCCAAGAGATGC-3' R: 5'-ACACTGTCTGCTGGTGGAGTTC-3'
<i>Il1b</i>	Interleukin 1 Beta	F: 5'-TGAAGTTGACGGACCCCAAA-3' R: 5'-TGATGTGCTGCTGTGAGATT-3'

<i>Inos</i>	Nitric Oxide Synthase 2	F: 5'-GGCAGCCTGTGAGACCTTTG-3' R: 5'-GAAGCGTTTCGGGATCTGAA-3'
<i>Lcn2</i> (Ngal)	Lipocalin 2, Neutrophil Gelatinase-Associated Lipocalin	F: 5'-GAAATATGCACAGGTATCCTC-3' R: 5'-GTAATTTTGAAGTATTGCTTGTTT-3'
<i>Mmp9</i>	Matrix Metalloproteinase 9	F: 5'-CCTGGAACTCACACGACATCTTC-3' R: 5'-TGGAAACTCACACGCCAGAA-3'
<i>Tgfb</i>	Transforming Growth Factor Beta	F: 5'-GCAACATGTGGAAGTCTACCAGA-3' R: 5'-GACGTCAAAGACAGCCACTCA-3'
<i>Timp1</i>	Tissue Inhibitor of Metalloproteinases 1	F: 5'-GTAAGGCCTGTAGCTGTGCC-3' R: 5'-AGGTGGTCTCGTTGATTCT-3'
<i>Tnfa</i>	Tumor Necrosis Factor Alpha	F: 5'-AAGCCTGTAGCCACGTCGTA-3' R: 5'-GGCACCAGTAGTTGGTTGTCTTTG-3'

Thermal Cycler Dice Real-Time Systems II (Takara Bio Inc., Shiga, Japan) was used to analyze mRNA expression in real time RT-PCR. The expression levels of each gene were normalized to *Gapdh* or *Actb* using the $\Delta\Delta CT$ comparison method.

2-4. Histology and immunostaining

Kidneys were fixed with 10% formalin and embedded in paraffin. Frozen samples were stored in OCT at -80 °C. Tissue sections (5 μ m thick) were stained with Periodic-acid Schiff (PAS) and Picrosirius Red according to standard protocols. To measure fibrosis, samples stained with Picrosirius Red were examined in 5 random fields under a polarizing microscope (Olympus IX73) and CellSens software (ver.1.12, Olympus, Tokyo, Japan). Tubular injury was indicated at PAS by necrotic lysis, tubular dilation, loss of the tubular brush border, cast formation, and detachment of cell debris into the tubule lumen. Grading was as previously described³¹, according to the following: normal as grade 0; < 25% as grade 1; 25%-49% as grade 2; 50%-74% as grade 3; and \geq 75% as grade 4.

Immunohistochemistry (IHC) of paraffin-embedded sections was performed to determine TIM-1/ KIM-1, F4/80, and smooth muscle actin α SMA in the kidney. Kidney sections

were deparaffinized, boiled in Target Retrieval Solution (Dako, Carpinteria, CA, USA), blocked with 2% normal goat serum, and reacted overnight with primary antibodies. Sections treated with anti-F4/80 antibody (BioRad), TIM-1/ KIM-1 (R&D), CD3 (Affymetrix) and Ly6G (BioLegend) were incubated with Histofine Simple Stain MAX PO (Nichirei Bioscience, Tokyo, Japan) followed by DAB Substrate Kit (Vector Laboratories, Burlingame, CA); sections treated with anti-actin, α SMA-AP (Sigma Aldrich, St.Louis, USA) were incubated with Alkaline Phosphatase Substrate-Vector Red (Vector Laboratories, Burlingame, CA). All sections were counterstained with hematoxylin. Species-matched immunoglobulin G (IgG) was used as a negative control for the primary antibodies. PAS, Picrosirius Red and IHC-stained sections were digitized using a microscope (FSX-100; Olympus). Fibrotic area and IHC-positive areas were quantified using ImageJ (Fiji, National Institute of Health, USA).

For immunofluorescence staining, the frozen sections were fixed, blocked, and incubated overnight with primary antibodies against CD206 (BioLegend), F4/80 (BioRad), CXCR3 (BD), and pTBK1 (Cell Signaling). The sections were then incubated with fluorochrome-conjugated secondary antibody (Thermo Fischer Scientific, Waltham, MA) and nuclear stain DAPI (Wako, Osaka, Japan). For co-staining with TUNEL, the In Situ Cell Death Detection Kit (Roche, Basel, Switzerland) was incubated at 37° for one hour. Species-matched IgG was used as a negative control for the primary antibodies. Images of the stained sections were digitized and analyzed using an FV1000 microscope (Olympus).

2-4. Live cell imaging

WT and *Aim2*^{-/-} mBMDMs were grown on collagen-coated glass-bottom dishes in serum-free RPMI1640 with Hoechst33342 and Sytox orange (Thermo Fisher Scientific), and induced to undergo pyroptosis with poly (dA:dT) using Lipofectamine 2000. Images

were taken using a fluorescent microscope FV1000 over a 2.5 h time course at 37°C in a 5% CO₂ atmosphere.

2-5. Western blot

Total protein lysates were prepared from the kidney using RIPA lysis buffer (20 mM Tris, 2.5 mM EDTA, 1% Triton X, 10% glycerol, 1% deoxycholic acid, 0.1% SDS, 50 mM NaF, and 10 mM Na₄P₂O₇-10H₂O) with protease inhibitors. Protein lysates of cells were obtained by direct addition of 5x Laemmli sample buffer to the wells containing both cells and supernatant to prevent loss of dead cells. Protein samples were denatured by boiling at 95°C for 8 min under reducing conditions and then subjected to SDS-PAGE. The protein bands were transferred to nitrocellulose membranes. The membranes were blocked with 5% skim milk or bovine serum albumin (BSA) buffer for one hour at RT and then incubated overnight at 4°C with the primary antibodies followed by one hour of incubation with the secondary antibodies conjugated to horseradish peroxidase (HRP). Western blot Quant HRP substrate or Ultra-Sensitive HRP substrate (Takara Bio Inc.) was used to detect the bands under Amersham Imager 680 (Cytiva, MA, USA). β -actin was the internal control for the loading amount of the protein. Primary antibodies against mouse AIM2 (Cell Signalling), GSDMD (Adipogen), N-terminal GSDMD (Cell Signalling), Caspase-1 (p20, Adipogen), IL-1 β (R&D), pIRF3 (Ser 396), pTBK1(Ser 172), STING, p-p65 (Ser 536, Cell Signalling), p65 (Santa Cruz Biotechnology, Dallas, TX, USA), and β -actin (Sigma) were used.

2-6. Flow cytometry

Flow cytometric analysis was performed as previously described³². In brief, mouse kidney was harvested, cut into small pieces, and digested in collagenase-D mixture (1 mg/mL collagenase D, 40 ng/mL DNase-I, 5 mM MgCl₂ in RPMI-1640) for 40 minutes at 37°C.

The tissue was pipetted to a homogeneous suspension and filtered through a 40- μ m cell strainer. After incubating the tissue in Ammonium-Chloride-Potassium (ACK) buffer to lyse the red blood cells, the cells were suspended with 40% Percoll and carefully plated onto 80% Percoll. After centrifugation, kidney leukocytes were layered between Percoll. The leukocytes were labeled with the following antibodies: FITC-conjugated anti-CD11b (BD Biosciences, CA, USA), 7-AAD (BD Biosciences), Brilliant Violet 421-conjugated anti-F4/80 (BioLegend), Brilliant Violet 510 -conjugated anti-CD45 (BD Biosciences). BD FACSVerse (BD Biosciences) was used for immunophenotype analysis, and FlowJo (ver10.6.0, Tree Star, Inc, CA, USA) was used for data analysis.

2-7. Serum chemistries

Serum levels of mice BUN, creatinine, and LDH were analyzed using the Fuji Dri-Chem analyzer (Fujifilm, Tokyo, Japan).

2-8. Picogreen assay

Blood was collected from the jugular vein of mice under anesthesia before and after glycerol injection. Plasma DNA content was measured using Quant-iT PicoGreen dsDNA reagent and kits (Thermo Fisher Scientific) according to the manufacturer's protocol. Fluorescence was measured using the SPARK 10M multimode microplate reader (TECAN, Switzerland).

2-9. BrdU incorporation analysis

Mice injected with glycerol were given a single intraperitoneal administration of 100 mg/kg 5-bromo-2-deoxyuridine (BrdU, Tocris Biosciences, Minneapolis, USA) 24 hours before sacrifice. After kidney collection, samples were fixed and embedded in paraffin. Five μ m paraffin-embedded sections were deparaffinized, cleared of antigens, blocked,

and incubated overnight with the primary antibody for BrdU (MBL). The following steps were similar to the immunofluorescence staining method mentioned above.

2-10. ELISA

The levels of TNF α , IFN- β , and Ccl2 in cell supernatant or/and tissue were measured using a mouse ELISA kit (R&D Systems, Minneapolis, MN, USA) according to the manufacturer's instructions.

2-11. Statistics

Data were expressed as mean \pm SD. An unpaired t-test was used to compare the two groups. For comparisons between multiple groups, the significance of differences between group means was determined by one-way analysis of variance (ANOVA) in combination with the Tukey-Kramer test or the Dunnett post hoc test. Two groups were compared using the paired or unpaired t-test. All analyses were performed using GraphPad Prism version 9 (San Diego, CA, USA). A p value of < 0.05 was considered statistically significant.

Chapter 3. Results

3-1. dsDNA was a potential DAMP during RIAKI.

To clarify the role of dsDNA in the pathophysiology of RIAKI, DNase-I, an extracellular dsDNA lysing endonuclease, was used in male WT mice with RIAKI. Injection of 5 mL/kg glycerol into the hindlimbs induced AKI in WT mice, but additional treatment with DNase-I restored renal function and inhibited inflammation and tubular injury. Serum BUN and creatinine levels were decreased (Fig. 2A, B), tubular injury and inflammation were ameliorated (Fig. 3A-D), and renal mRNA levels of KIM-1 and Ngal were alleviated by DNase-I treatment in WT mice ingested with glycerol (Fig. 3D, F), whereas serum LDH levels, an indicator of muscle damage, were unaffected (Fig. 2C). Overall, these results suggest that dsDNA is a potential DAMP during RIAKI.

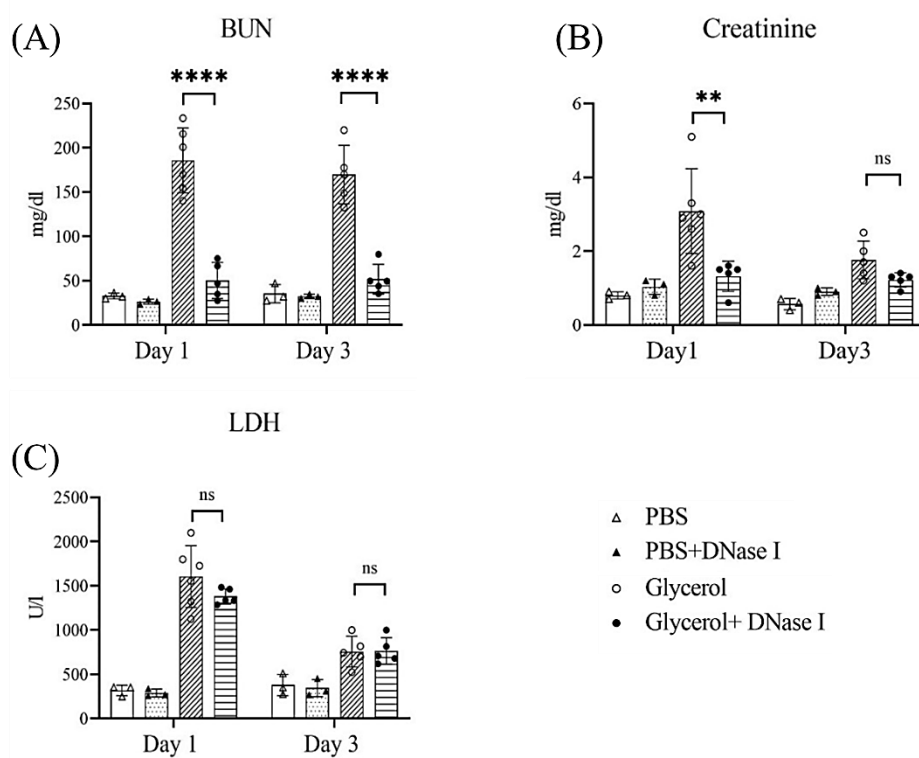


Figure 2. DNase-I improved RIAKI

DNase-I was administered peritoneally just before and after glycerol injection and every 12 h thereafter in WT mice. (A) Serum levels BUN, (B) creatinine, and (C) LDH levels on day 1 and day 3 (n = 3 for each control group, n = 5-6 for the glycerol injection group with or without DNase-I treatment group). Data are expressed as mean \pm SD. **p < 0.01 and ****p < 0.0001

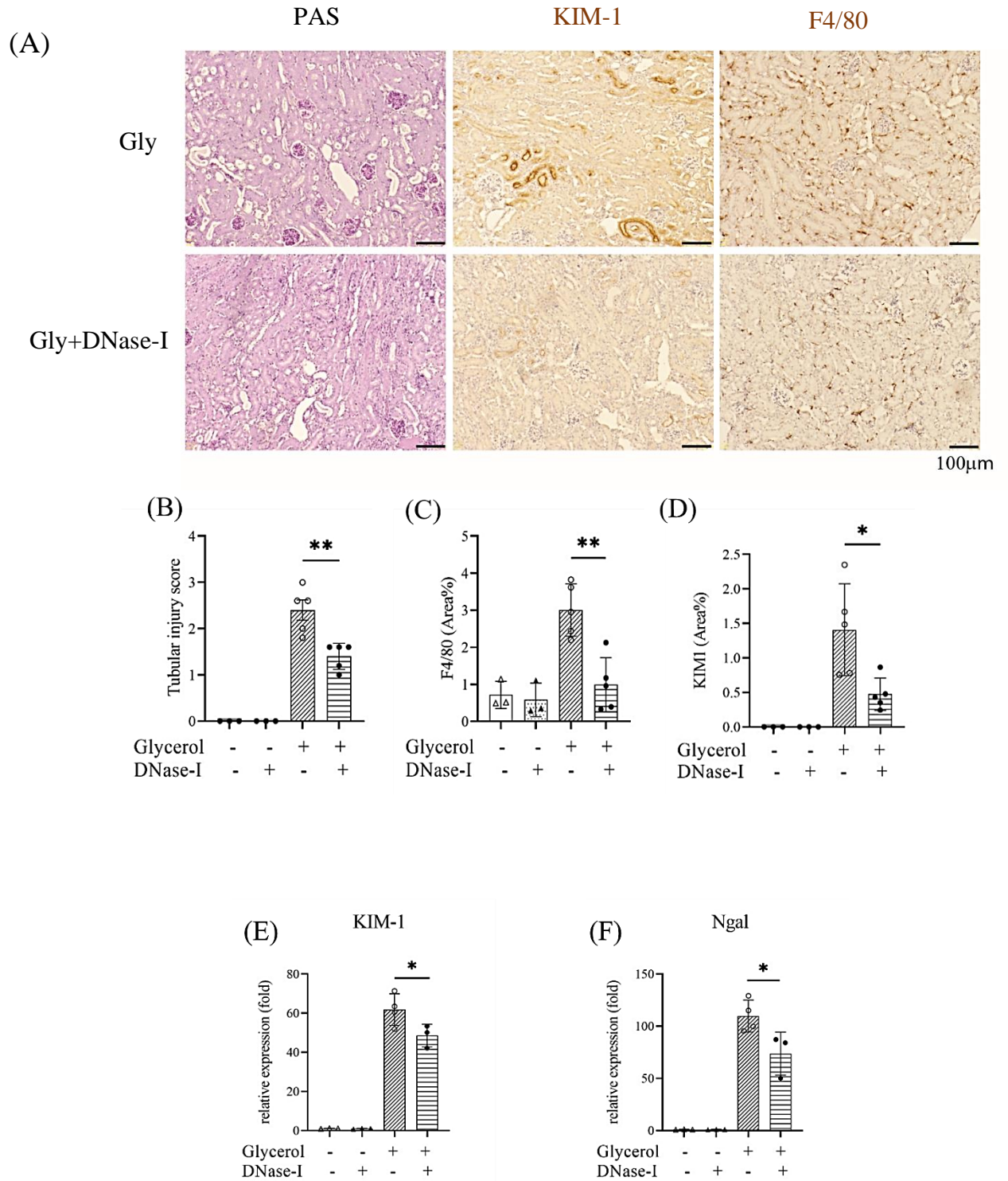


Figure 3. DNase-I ameliorated tubular injury and inflammation during RIAKI. (A) PAS staining, immunohistochemistry for KIM-1 and F4/80 in kidneys on day 3 after glycerol injection. Representative images were shown. (B) Semi-quantitative assessment of tubular injury on PAS-stained sections (n = 5 mice per group) (C) F4/80- and (D) KIM-1-positive areas were quantified (n=5 mice per group). (E) KIM-1 and (F) Ngal mRNA expression in kidney was analyzed by real-time PCR (n = 3-4 mice per group). Data are expressed as mean \pm SD. *p < 0.05 and **p < 0.01

3-2. *Aim2*^{-/-} mice delayed recovery without disturbing tubular cells.

As mentioned earlier, AIM2 is expressed in tubular cells, podocytes in the glomerulus, and interstitial macrophages in the kidney. In order to clarify the function of AIM2 during RIAKI, we generate *Aim2*^{-/-} mice using CRISPR/Cas9 knockout system on C57BL/6J background mice (Fig. 4). The *Aim2*^{-/-} phenotype was confirmed by experiments using mBMDM (Fig. 5). Lipofectamine was used to transfect dsDNA into cells. IL-1 β , product of inflammasome activation was released after dsDNA transfection in WT-mBMDMs. At the same time point, *Aim2*^{-/-} mBMDMs did not induce IL-1 β secretion after dsDNA treatment (Fig. 5A, B).

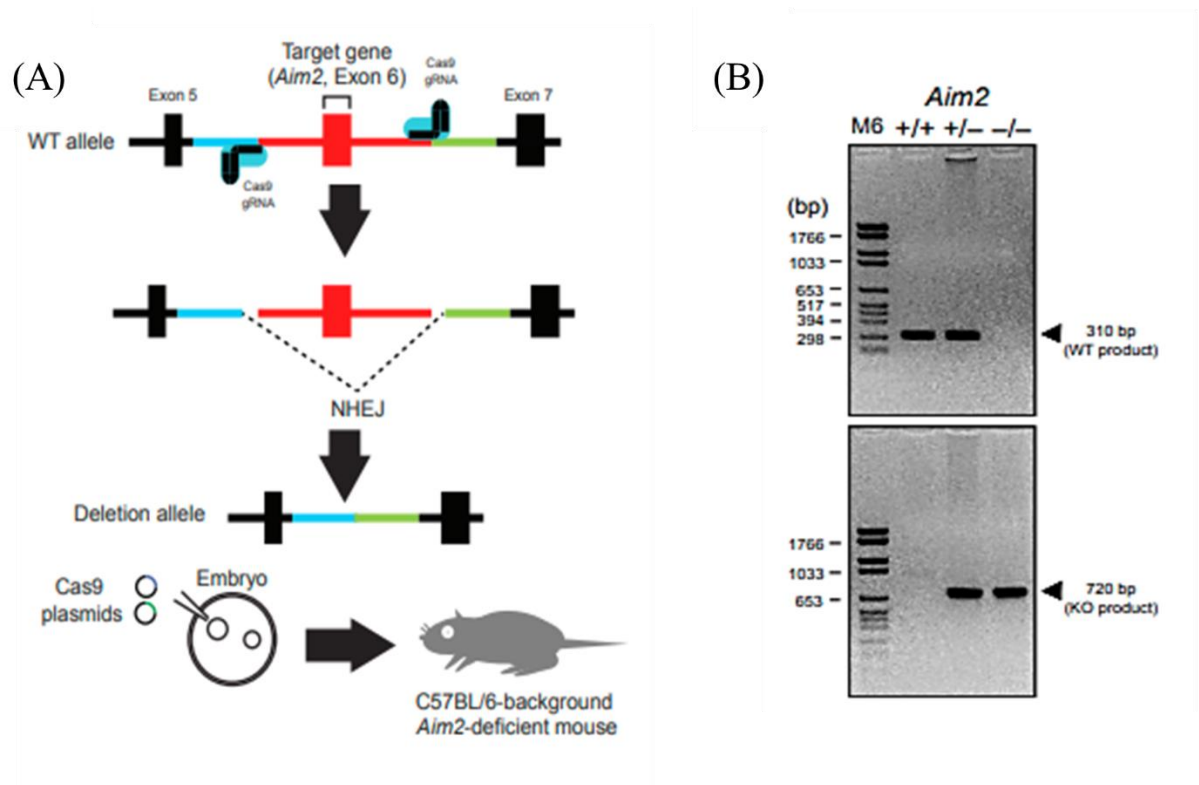


Figure 4. Generation of *Aim2*^{-/-} mice and genotyping

(A) *Aim2*^{-/-} mice were generated by CRISPR-Cas9 based genome editing. The exon 6 of murine *Aim2* was targeted for deletion. Embryos were transferred to C57BL/6 female mice. (B) Genomic DNA was isolated from mouse tail samples. *Aim2*^{-/-} mice were genotyped using PCR: Representative 310-bp WT DNA products and 720-bp mutant DNA products are shown.

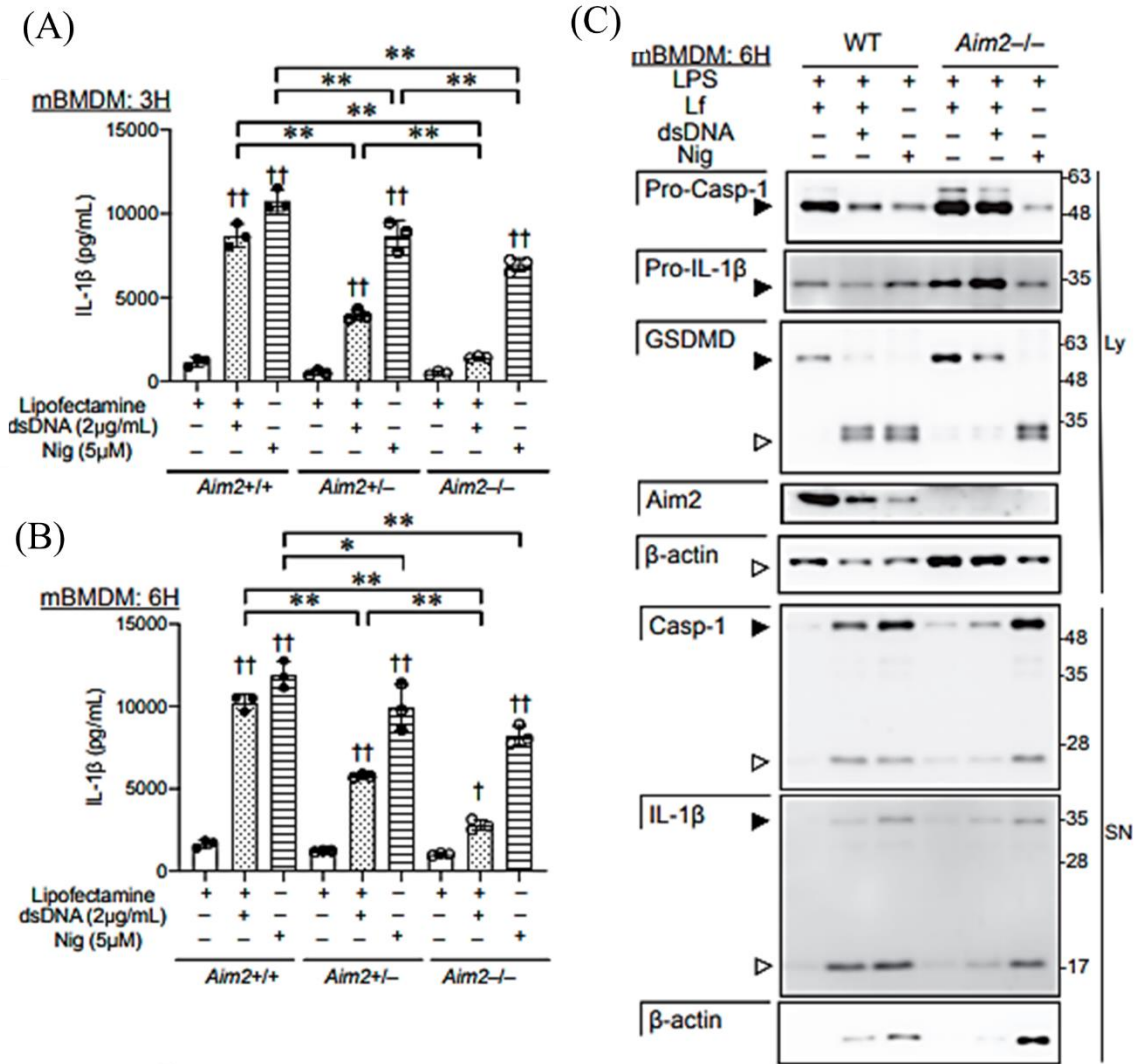


Figure 5. Confirmation phenotypes of *Aim2*^{-/-} mice.

(A-C) bone marrow-derived macrophages (mBMDMs) were isolated from WT and *Aim2*^{-/-} mice. LPS-primed mBMDMs were treated with Lipofectamine 2000 with or without 2 μ g/mL dsDNA or 5 μ M nigericin (Nig) for 3 or 6 hours. (A and B) IL-1 β secretion was measured in supernatants 3 or 6 hours after treatment. (C) Immunoblotting for caspase-1, IL-1 β , gasdermin D, AIM2, and β -actin was performed. (Ly=Lysate; SN=supernatant) * p < 0.05 and ** p < 0.01. † p < 0.05 and †† p < 0.01 vs. controls at day 0

After 6 hours of dsDNA exposure, inflammasome-related proteins, such as N-terminal GSDMD, cleaved Casp-1, mature IL-1 β , were detected in WT mBMDMs, but the detection levels were extremely lower in *Aim2*^{-/-} mBMDMs. However, in both LPS-primed WT and *Aim2*^{-/-} macrophages, cleaved Casp-1, GSDMD and pro-IL-1 β did not change by treatment with nigericin (NLRP3 inflammasome activator) (Fig. 5C).

To investigate the role of AIM2 in RIAKI, we injected glycerol into *Aim2*^{-/-} mice. Plasma dsDNA increased equally in both WT and *Aim2*^{-/-} mice within one hour (Fig. 6A). Even 72 hours after glycerol injection, the increase in plasma dsDNA was maintained in both WT and *Aim2*^{-/-} mice. Plasma LDH levels, indicating muscle damage, were also detected at the same levels at all time points between WT and *Aim2*^{-/-} mice (Fig. 6B). Interestingly, the BUN levels were higher in the *Aim2*^{-/-} mice than those in the WT mice at later time points from day 3 to 28 after glycerol injection (Fig. 7A). This persistent elevation of BUN levels indicates delayed recovery from renal injury in *Aim2*^{-/-} mice.

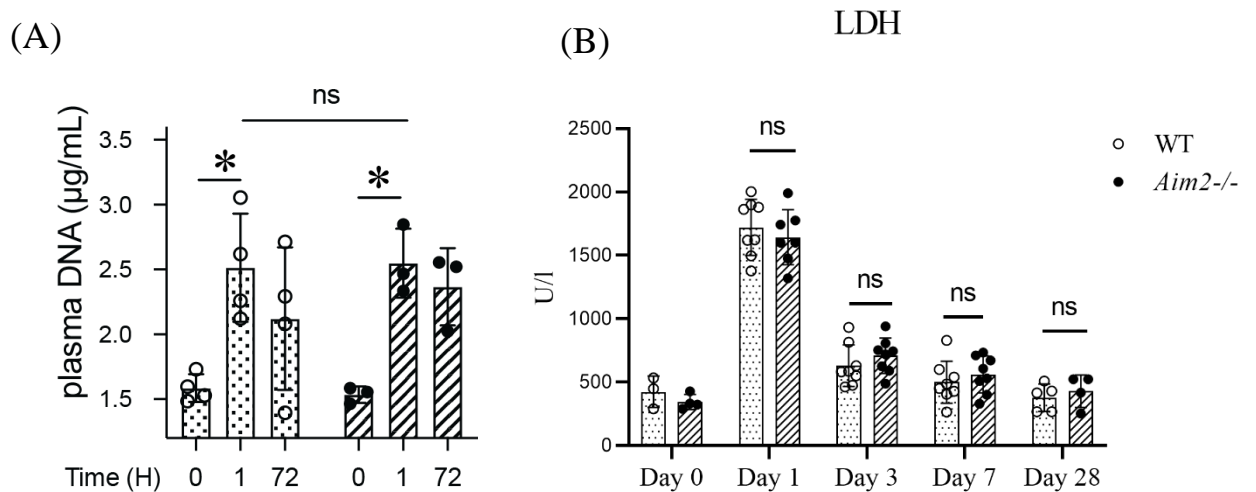


Figure 6. *Aim2*^{-/-} did not affect muscle injury after glycerol injection. Plasma dsDNA was measured (n = 4,4,4 for WT mice, n = 3,3,3 for *Aim2*^{-/-}). (B) LDH were measured (n = 3,8,8,8,5 for WT, n = 4,7,8,8,4 for *Aim2*^{-/-}). Data are expressed as mean ± SD. *p < 0.05.

Although the levels of BUN and creatinine were higher in the later stage of RIAKI in *Aim2*^{-/-} mice, the glomeruli were intact and tubular injury was similar in WT and *Aim2*^{-/-} mice when histology was assessed by PAS staining (Fig. 7B, C) and mRNA levels of KIM-1 or Ng2 were assessed by RT-PCR (Fig. 7D, E). These results suggest that deletion of AIM2 prolonged the healing process after kidney damage without affecting tubular cells or glomeruli.

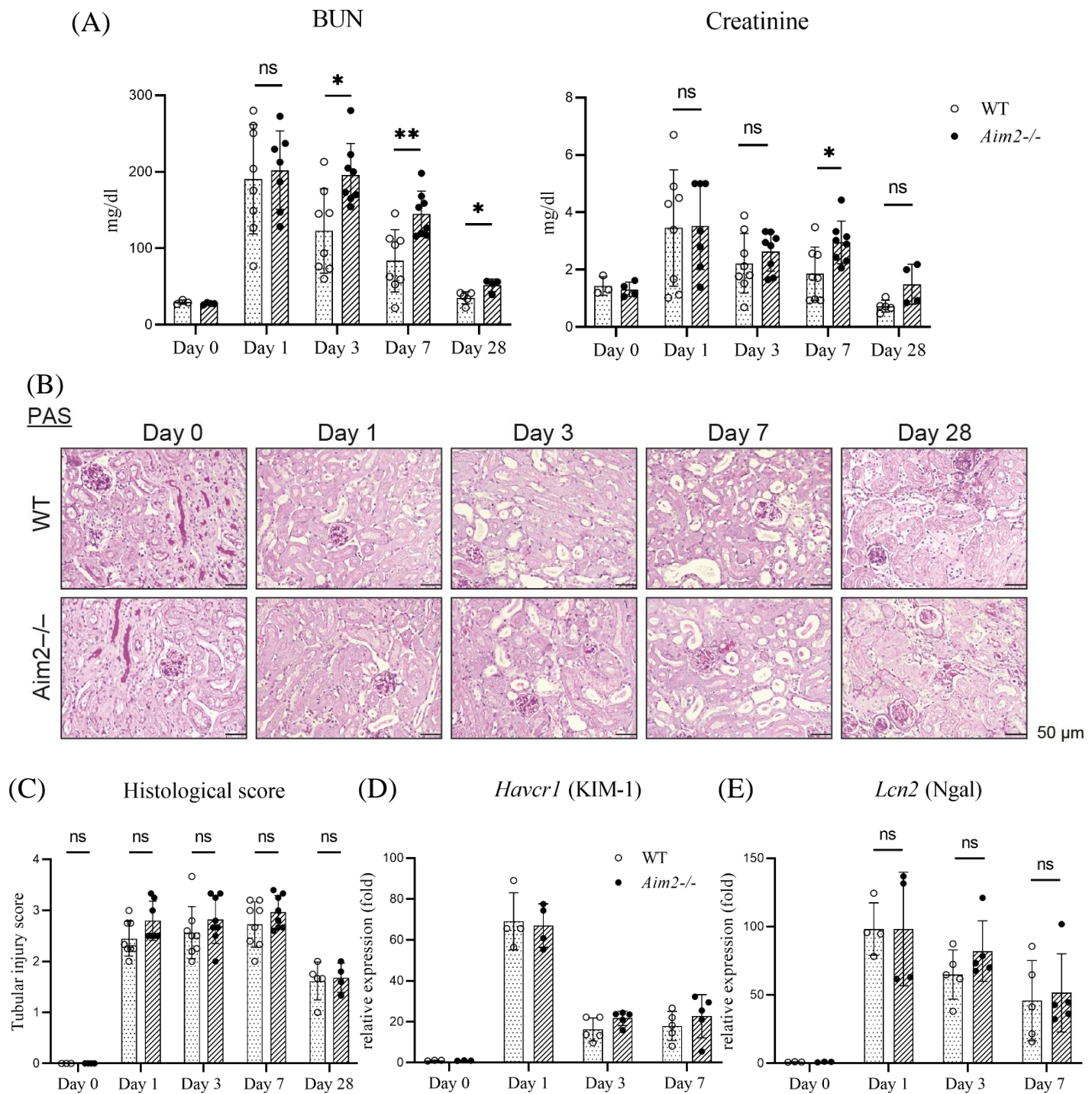


Figure 7. *Aim2*^{-/-} delayed recovery but tubular injury was similar.

(A) Serum BUN and creatinine were measured (n = 3,8,8,8,5 for WT, n = 4,7,8,8,4 for *Aim2*^{-/-}) and (B) PAS staining of kidney samples from WT mice and *Aim2*^{-/-} mice was used to assess renal tubular injury. Representative images were shown. (C) Semi-quantitative analysis of tubular injury (n = 3,8,8,8,5 for WT, n = 4,7,8,8,4 for *Aim2*^{-/-}). (D) Kidney mRNA expressions of KIM-1 and (E) Ngal were analyzed in real time RT-PCR (n = 3-5 mice for each time point). Data are expressed as mean \pm SD. *p < 0.05 and **p < 0.01.

3-3. *Aim2*^{-/-} exacerbated renal fibrosis after RIAKI.

If recovery is altered, AKI can lead to CKD by fibrosis regardless of etiology⁵⁸. To investigate the fibrosis, we performed Picrosirius red staining under polarizing microscope, which provides detailed information to distinguish the collagen subtypes of the fibrotic area, including collagen type I (red), collagen type III (green). In addition to the higher BUN level in *Aim2*^{-/-} mice, glycerol injection resulted in a strong accumulation of collagen type I and III in *Aim2*^{-/-} mice compared to WT mice from day 3 to 28 (Fig. 8A-C).

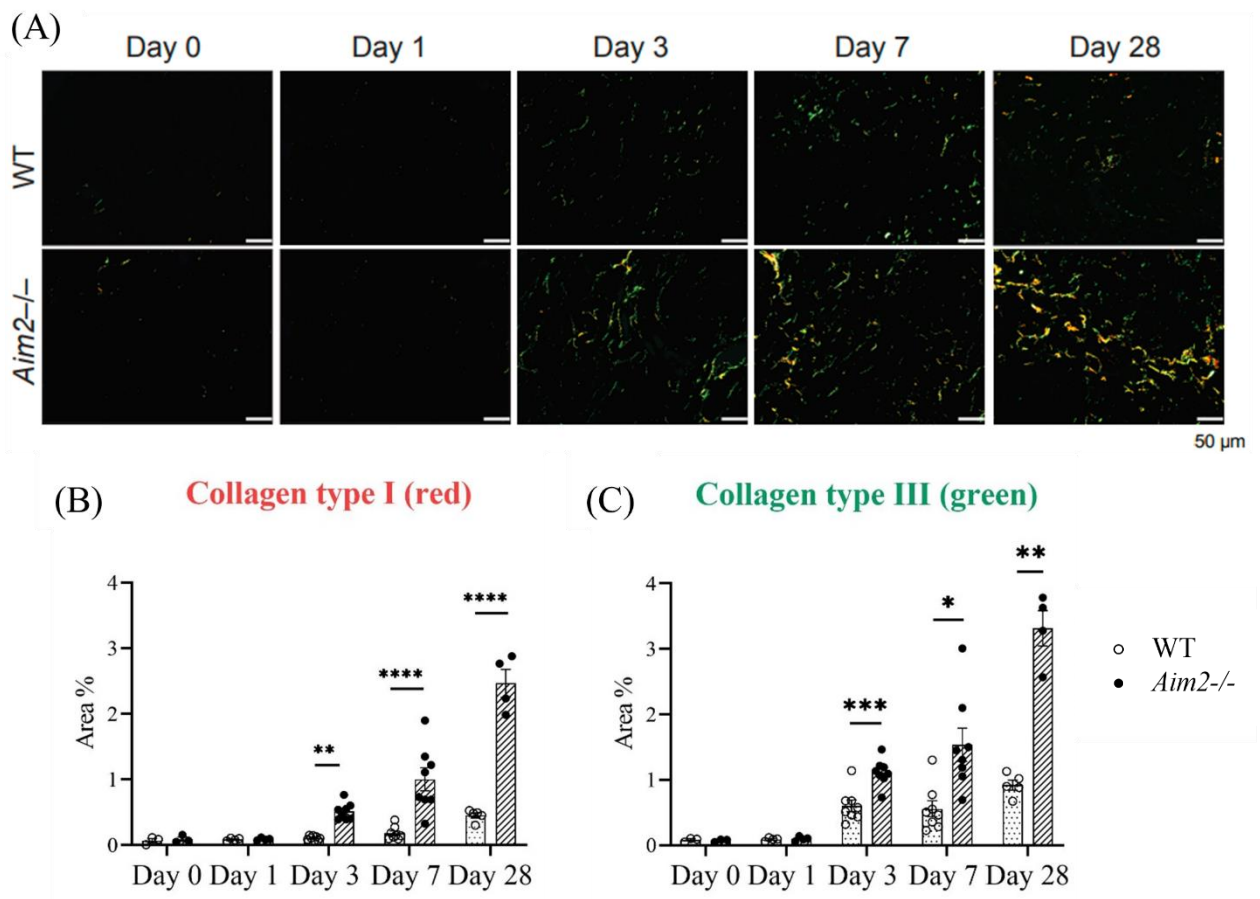


Figure 8. *Aim2*^{-/-} increased collagen accumulation after RIAKI.

(A) Picrosirius red staining in the kidney cortex of WT and *Aim2*^{-/-} mice were observed under polarized microscopy. Representative images shown. (B) Collagen type I (red) (C) Collagen type III (green) were quantified (n = 3,8,8,8,5 for WT, n = 4,7,8,8,4 for *Aim2*^{-/-}). Data are expressed as mean ± SD. *p<0.05, **p<0.01, ***p<0.001 and ****p<0.0001.

The mRNA levels of fibrosis markers such as *Tgfb*, *Colla1*, *Timp1* and *Mmp9*, were also expressed more in *Aim2*^{-/-} mice compared to those in WT mice (Fig. 9A).

Furthermore, IHC for α SMA (Fig. 9B) showed that the positive area was significantly higher in *Aim2*^{-/-} mice than that in WT mice at day 7 after glycerol injection (Fig. 9C), confirming above-mentioned findings that AIM2 deficiency led to progressive renal fibrosis after RIAKI.

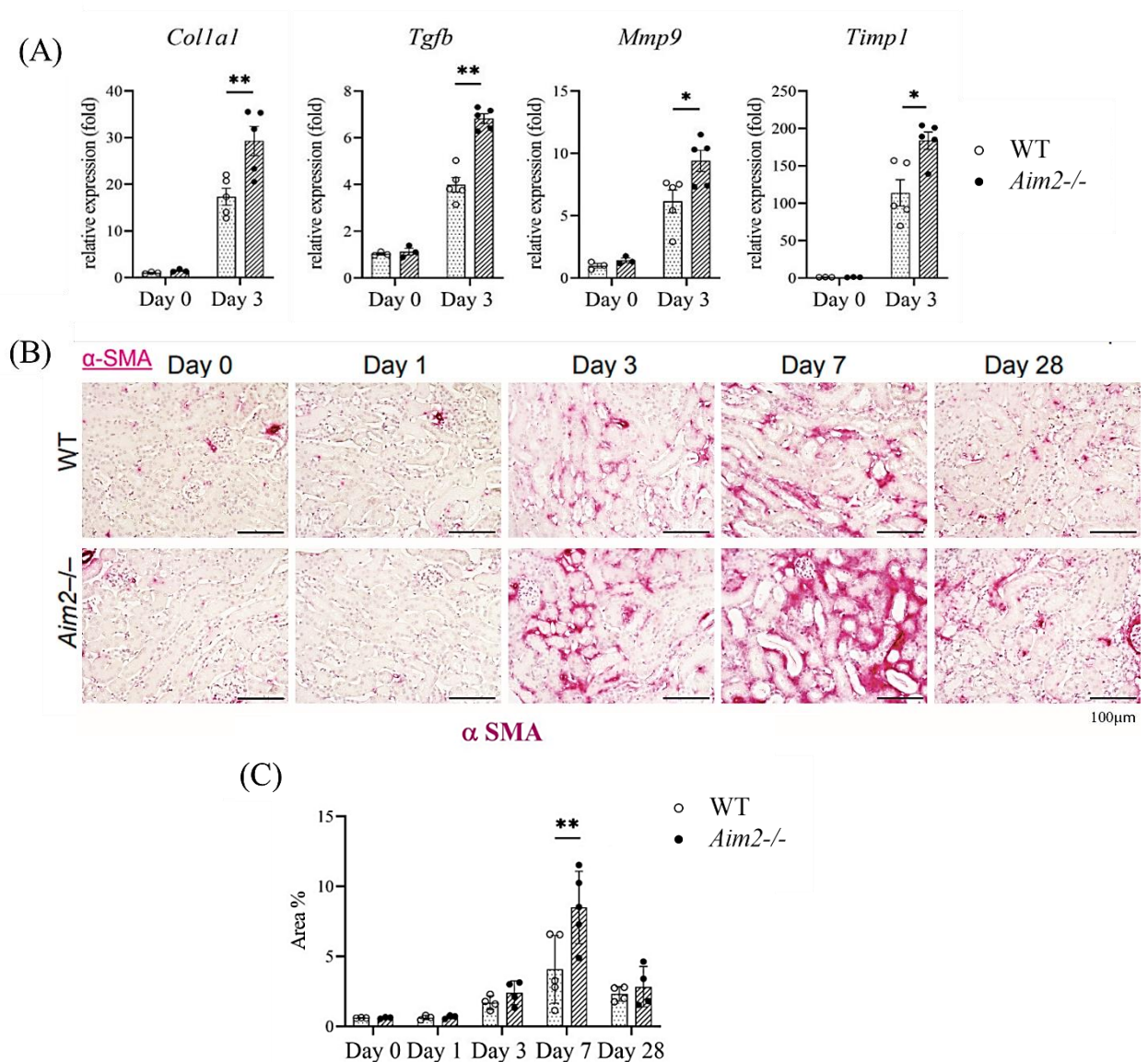


Figure 9. *Aim2*^{-/-} accelerated fibrosis after RIAKI.

(A) Fibrosis markers (*Colla1*, *Tgfb*, *Mmp9*, *Timp1*) were measured (n = 3,5 for both WT and *Aim2*^{-/-}), (B) Immunohistochemical staining of α SMA. Representative image shown. (Day 0, 1, 3, 7, and 28) (C) Quantification of α SMA (n = 3,3,4,5,4 for both WT and *Aim2*^{-/-}). Data are expressed as mean \pm SD. *p<0.05, **p<0.01.

3-4. Macrophages accumulated in *Aim2*^{-/-} kidney during RIAKI.

Our results showed delayed recovery with excessive fibrosis in *Aim2*^{-/-} mice at later time points of RIAKI progression. However, these findings were not related to both tubular cells and glomeruli (Fig. 7).

RIAKI is a sterile renal inflammation caused by DAMPs released from damaged muscles. Therefore, components of adaptive or innate immunity are essential for this process. To find the cells responsible for severe fibrosis during the RIAKI of *Aim2*^{-/-} mice, we examined the expression of markers of lymphocytes, neutrophils, and macrophages in WT and *Aim2*^{-/-} mice after RIAKI.

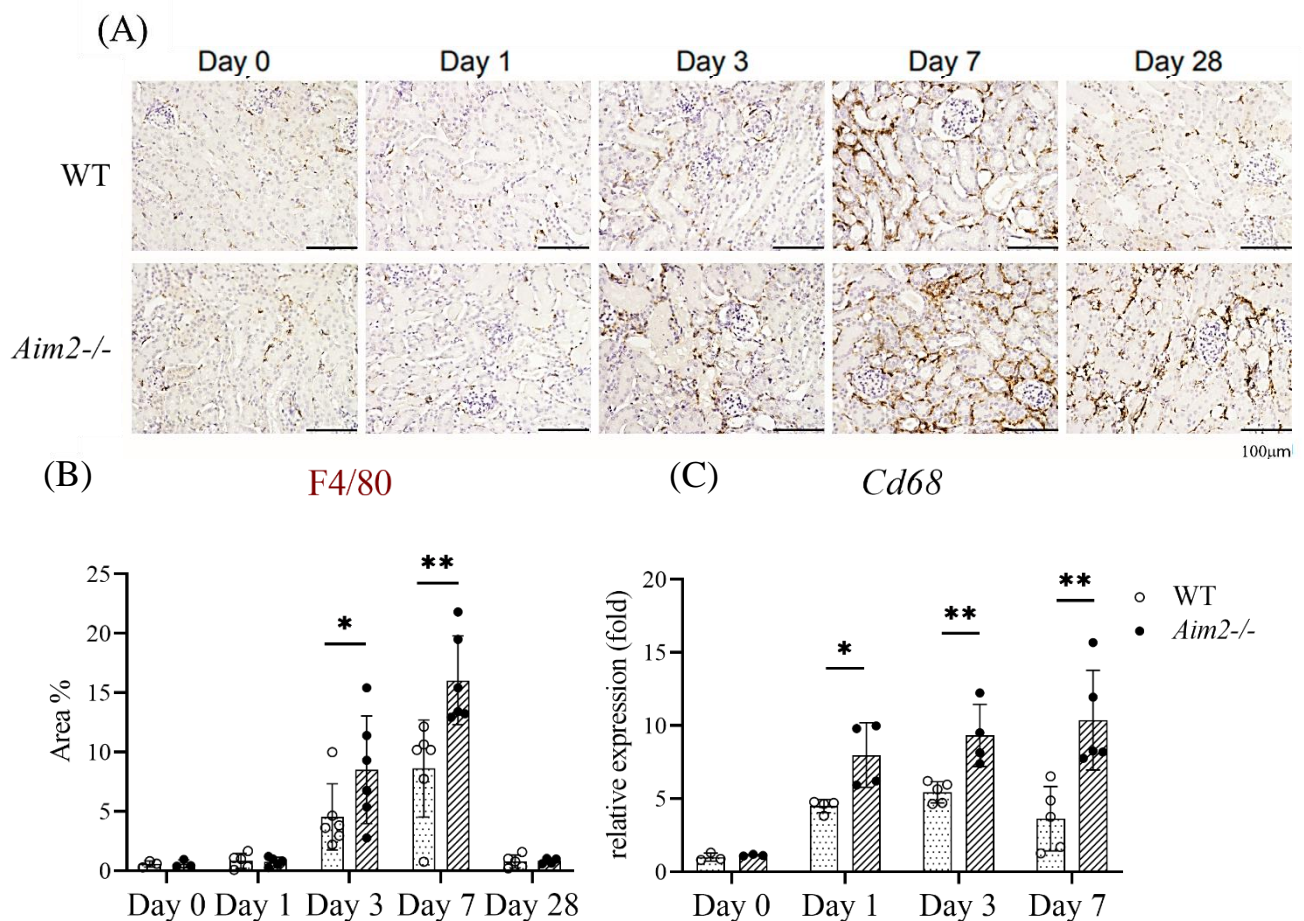


Figure 10. Macrophages accumulated in *Aim2*^{-/-} kidneys during RIAKI.

(A) Immunohistochemistry of F4/80 was performed on kidney sections after RIAKI. Representative images are shown. (B) Semi-quantitative evaluation of F4/80+ cells in kidney (n = 3,5,6,6,5 for WT, n = 3,5,6,6,4 for *Aim2*^{-/-}). (C) *Cd68* in total kidney lysate was analysed using RT-PCR. (n = 3–5 mice for each group). Data are expressed as mean ± SD. *p<0.05, **p<0.01.

IHC showed a sustained accumulation of F4/80 macrophages in the WT kidney after glycerol injection, and *Aim2*^{-/-} showed greater amounts of macrophages than WT on days 3 and 7 (Fig. 10A, B). Also, the mRNA level of *Cd68* (pan-macrophage marker) was more upregulated in *Aim2*^{-/-} mice than that in WT mice (Fig. 10C).

In addition, we found that M2 macrophages were more accumulated in the *Aim2*^{-/-} kidney, as shown by immunofluorescence staining of CD206 and mRNA expression of *Arg-1* and *Cd206* (Fig. 11 A, B, D, E). In contrast, mRNA expression of *Inos*, the marker of inflammatory classically activated macrophages (M1 macrophages), was downregulated and expressed comparably in WT and *Aim2*^{-/-} mice (Fig. 11C).

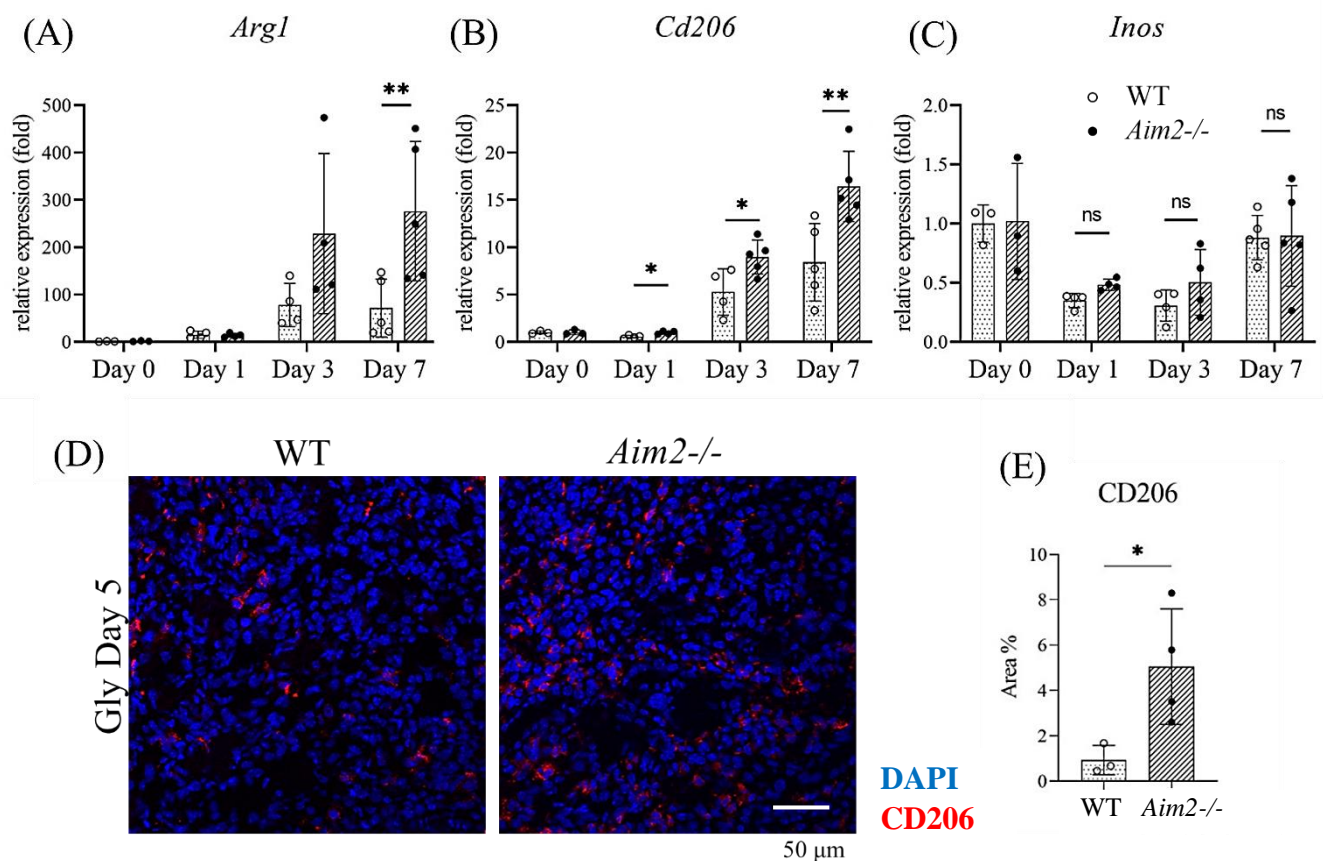


Figure 11. M2 macrophages were dominant during RIAKI. mRNA levels of (A) M2 marker *Arg1* and (B) *Cd206* and (C) M1 marker *Inos* were measured. (D) Immunofluorescent representative images of CD206 were performed on kidney sections after RIAKI. (E) Semi-quantitative evaluation of F4/80⁺ cells in kidney (n = 3 for WT, n = 4 for *Aim2*^{-/-}). Data are expressed as mean ± SD. *p < 0.05, **p < 0.01.

Next, several common chemokine receptors were assessed to learn more about the accumulated cells in the injured kidney of *Aim2*^{-/-} mice. *Ccr2*, *Ccr5* and *Cxcr3* were upregulated during RIAKI (Fig. 12A). While the expression of *Ccr2* and *Ccr5* was similarly increased in both WT and *Aim2*^{-/-} kidney, *Cxcr3* was specifically upregulated in *Aim2*^{-/-} kidney. CXCR3 is expressed by T cells, natural killer (NK) cells, dendritic cells, and macrophages⁵⁹. Immunofluorescence staining showed that most CXCR3⁺ cells were co-stained with CD206 (Fig. 12B).

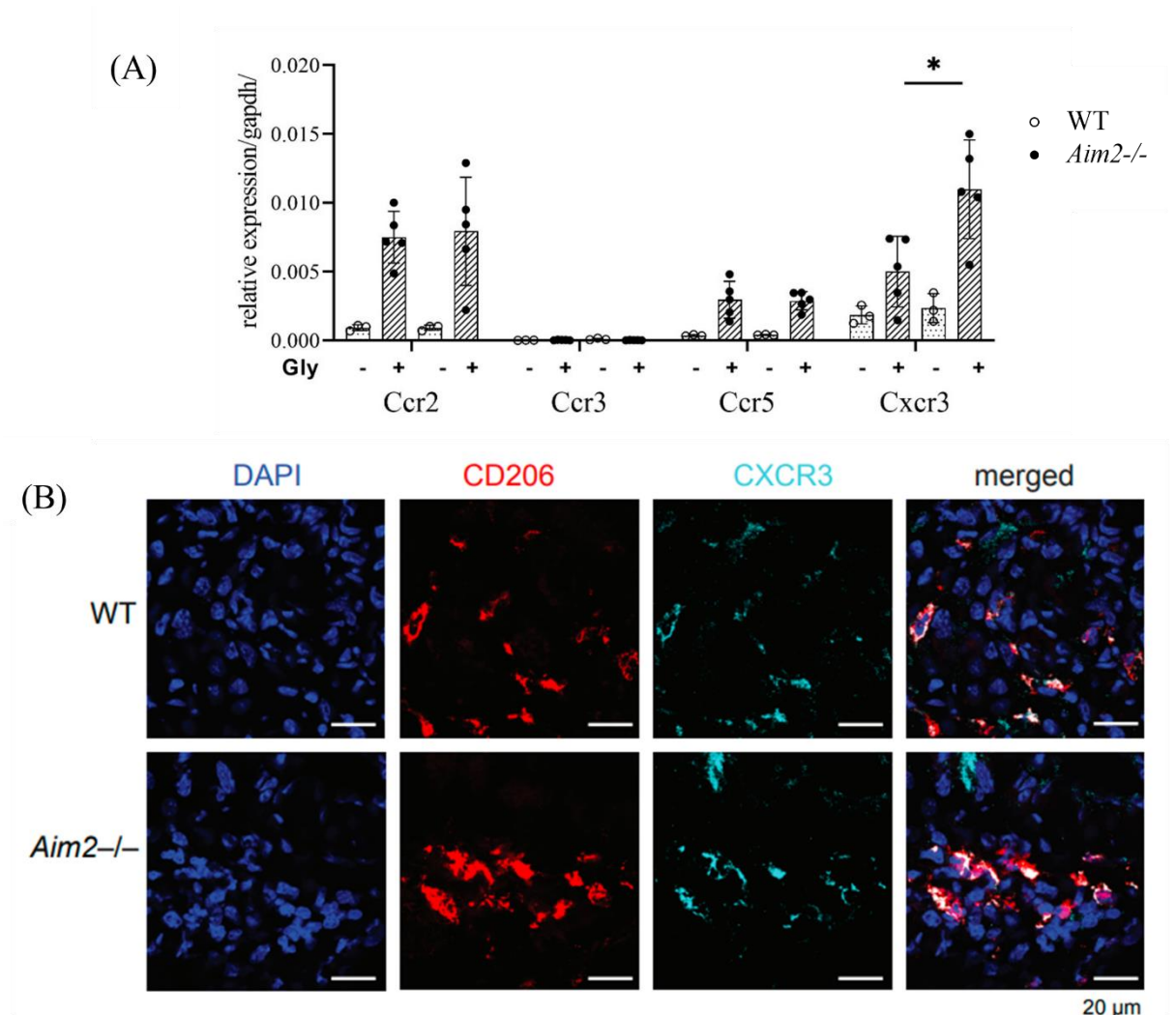


Figure 12. CXCR3 signaling contributed macrophage infiltration during RIAKI. (A) Leukocyte markers *Ccr2*, *Ccr3*, *Ccr5*, and *Cxcr3* in the kidneys 7 days after RIAKI were assessed by real-time RT-PCR (n = 3–5 mice for WT and *Aim2*^{-/-}) (B) Immunofluorescent staining for CXCR3 and F4/80 cells was performed on the kidney sections 7 days after RIAKI. Data are expressed as mean ± SD. *p<0.05.

These results suggest that excessive infiltration of M2 macrophages could be mediated by CXCR3 signaling in *Aim2*^{-/-} kidney during RIAKI.

To determine contribution of lymphocytes and neutrophils during RIAKI, we performed IHC staining for CD3 and Ly6G on day 3 samples. CD3-positive cells were not detected, and a few Ly6G-positive cells were found in the kidney of both WT and *Aim2*^{-/-} mice (Fig. 13A). Moreover, the mRNA levels of *Foxp3* in the kidney of WT and *Aim2*^{-/-} mice were very similar from day 1 to day 7 (Fig. 13B).

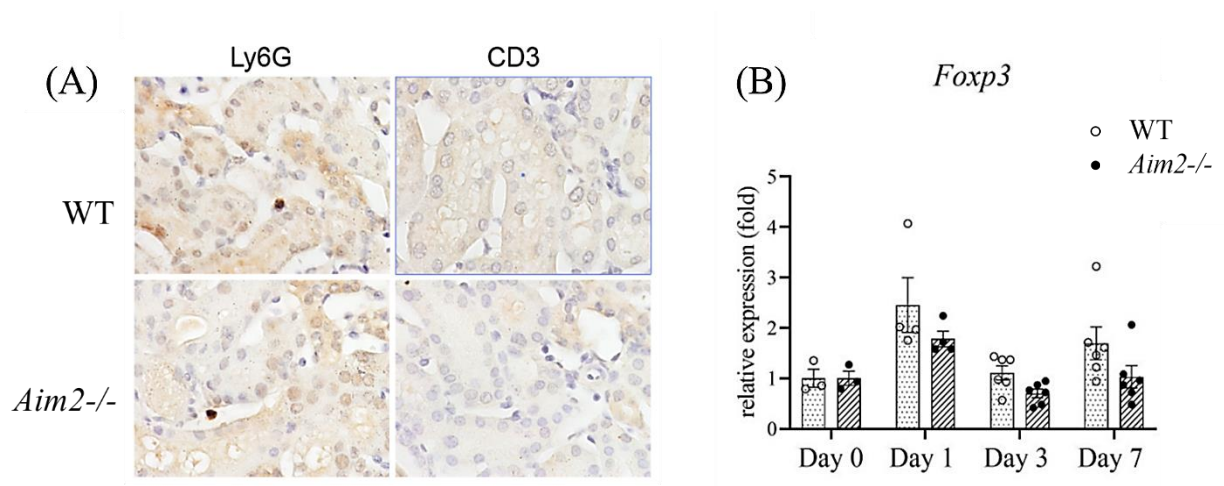


Figure 13. Neutrophils and lymphocytes played minor role during RIAKI. (A) Immunohistochemistry for Ly6G and CD3 were stained in day 3 samples from WT and *Aim2*^{-/-} mice. (B) *Foxp3* was measured using real time RT-PCR. (n = 3,4,6,6 for each WT and *Aim2*^{-/-}). Data are expressed as mean ± SD.

These results suggest that T cells and neutrophils have minor contribution during RIAKI but M2 macrophages are involved in severe fibrosis in *Aim2*^{-/-} mice at the later stage of RIAKI.

3-5. Deletion of *Aim2* did not affect cell proliferation during RIAKI

AIM2 reportedly regulates cell proliferation, especially in cancer cells^{60,61}. Therefore, we assessed cell proliferation in the kidney after glycerol injection using the bromodeoxyuridine (BrdU) assay. BrdU incorporates DNA of dividing cells and is widely used to assess cell proliferation *in vivo* and *in vitro*. The cell nuclei stained with BrdU were comparable between WT and *Aim2*^{-/-} mice at day 3. Therefore, we concluded that AIM2 had no effect on cell proliferation and regeneration during RIAKI. (Fig. 14).

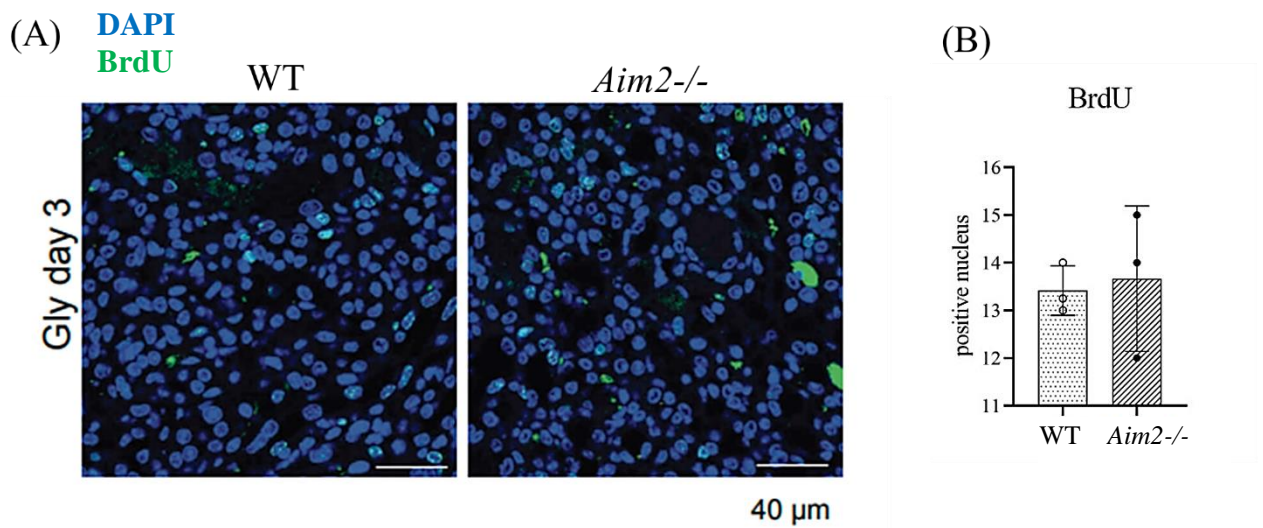


Figure 14. Kidney BrdU incorporation analysis after glycerol injection
WT and *Aim2*^{-/-} subjected to glycerol-induced RIAKI. 10mg/ml BrdU was intraperitoneally injected to mice 24-hours before harvesting kidneys. (A) Immunostaining for BrdU was performed on paraffin-embedded sections of the kidneys. (B) BrdU positive nuclei were counted.

3-6. Macrophage pyroptosis was restricted but NF- κ B was activated in *Aim2*^{-/-} mice kidney during RIAKI.

Macrophages are the immune cells responsible for controlling the process of RIAKI⁴⁷.

To allow normal healing process after the onset of RIAKI, different macrophage subtypes should be in balance. Our previous results showed that M2 macrophages were increased in the kidney of *Aim2*^{-/-} mice after RIAKI, which may be related to excessive fibrosis, leading to CKD. Therefore, we next investigated how M2 macrophages were increased in the kidney of *Aim2*^{-/-} mice during RIAKI.

First, we assessed the cell death of macrophages using flow cytometry (Fig. 15), because macrophages may undergo AIM2-pyroptosis induced by dsDNA during RIAKI.

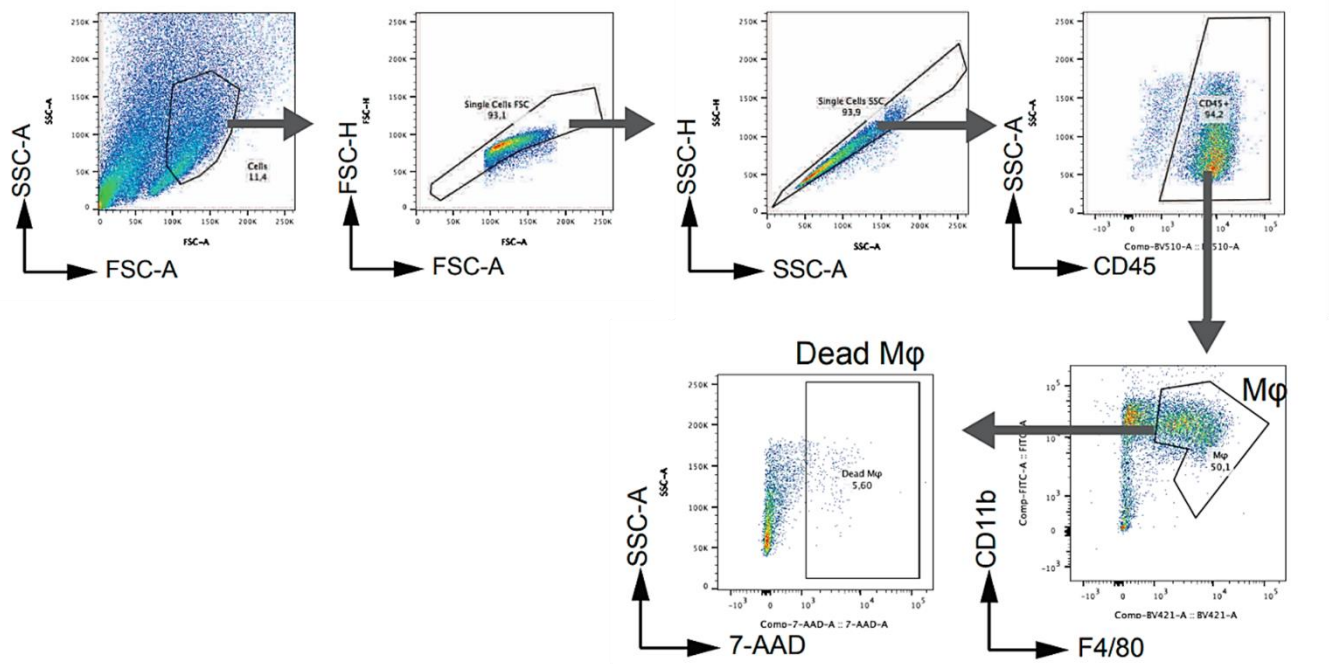


Figure 15. Flow cytometric analysis for cell death of macrophages in kidney. Glycerol injected WT and *Aim2*^{-/-} mice were analyzed. Shown is the gating strategy for macrophage cell death.

At 5 days after induction of rhabdomyolysis, more dead macrophages were counted in the kidney of WT than that of *Aim2*^{-/-} mice (Fig. 16A). Consistently, more TUNEL-positive F4/80⁺ macrophages were found in the kidney of WT mice (Fig. 16B).

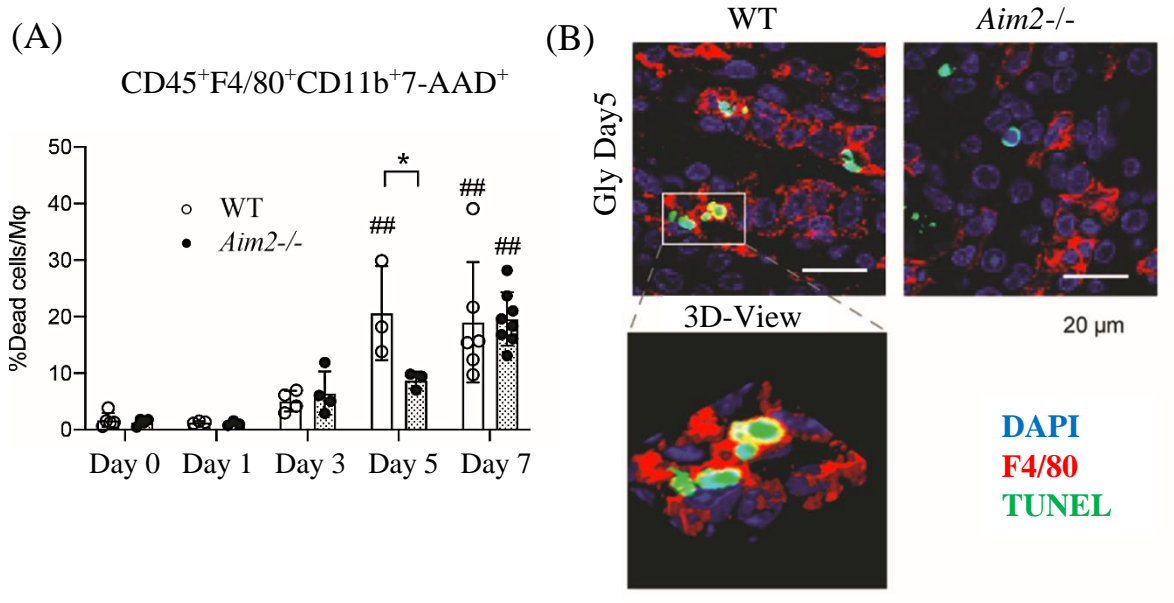


Figure 16. Cell death of macrophages is less in *Aim2*^{-/-} mice kidney. (A) Flow cytometric analysis for detecting CD45⁺F4/80⁺CD11b⁺7-AAD⁺ cells in WT and *Aim2*^{-/-} mice after glycerol injection (n = 3–8 for each; mean ± SD; *p < 0.05; ##p < 0.01 vs controls at Day 0). (B) Immunofluorescent staining for F4/80 (red) and TUNEL (green) in WT and *Aim2*^{-/-} kidneys 5 days after RIAKI.

These findings showed that macrophages died in the kidney of WT mice, although neither TUNEL staining, nor flow cytometry are specific to detect pyroptosis.

To assess inflammasome activation and pyroptosis during RIAKI, we injected glycerol into ASC-citrine mice which express fluorescent ASC to assess the formation of inflammasome assembly. In response to glycerol injection, ASC specks were formed in F4/80⁺ macrophages at day 5 in ASC-citrine mice (Fig. 17A). In addition, western blot analysis showed that N-terminal GSDMD (an executor of pyroptosis) was detected in WT mice but was reduced in *Aim2*^{-/-} mice (Fig. 17B, C). These

findings suggest that deletion of *Aim2* reduces pyroptosis of macrophages after glycerol injection.

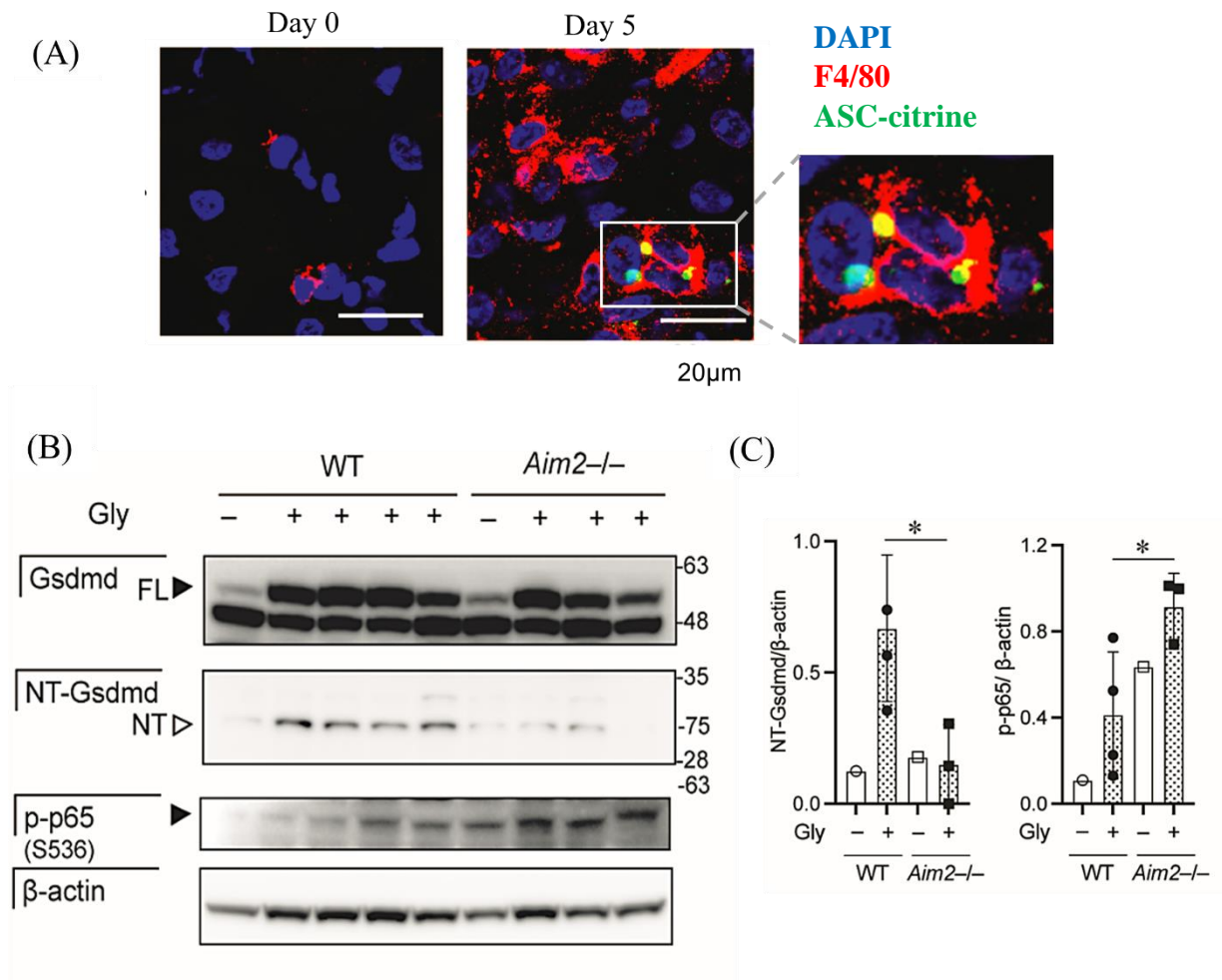


Figure 17. *Aim2*^{-/-} restricted macrophage pyroptosis during RIAKI.

(A) Immunofluorescent staining for F4/80 (red) in ASC-Citrine mice 5 days after glycerol injection. ASC-Citrine aggregates are shown in green. (B) Kidney expression of Gsdmd, cleaved amino-terminal (NT)-Gsdmd, and phosphorylated NF-κB p65 subunit (p-p65; Serine 536) was assessed by immunoblotting. (C) Semi-quantitative analysis of immunoblotting for NT-Gsdmd and p-p65 was performed. β-actin was used as the internal control (n = 3-4 for WT and 3 for *Aim2*^{-/-}) mean ± SD; *p < 0.05.

Along with restricted macrophage pyroptosis, we assessed inflammatory responses in WT and *Aim2*^{-/-} kidneys during RIAKI. Interestingly, reduced pyroptotic cell death on *Aim2*^{-/-} macrophages was not related to the phosphorylation of nuclear factor-κB (NF-κB) p65 subunit (Fig. 17B). Moreover, higher amounts of inflammatory cytokines TNFα and IFNβ were produced in RIAKI kidney of *Aim2*^{-/-} mice (Fig.

18C). Also, TANK-binding kinase (TBK1), a non-canonical NF- κ B activator, was phosphorylated in the cytoplasm of F4/80⁺ macrophages in *Aim2*^{-/-} mice kidney (Fig. 18A, B).

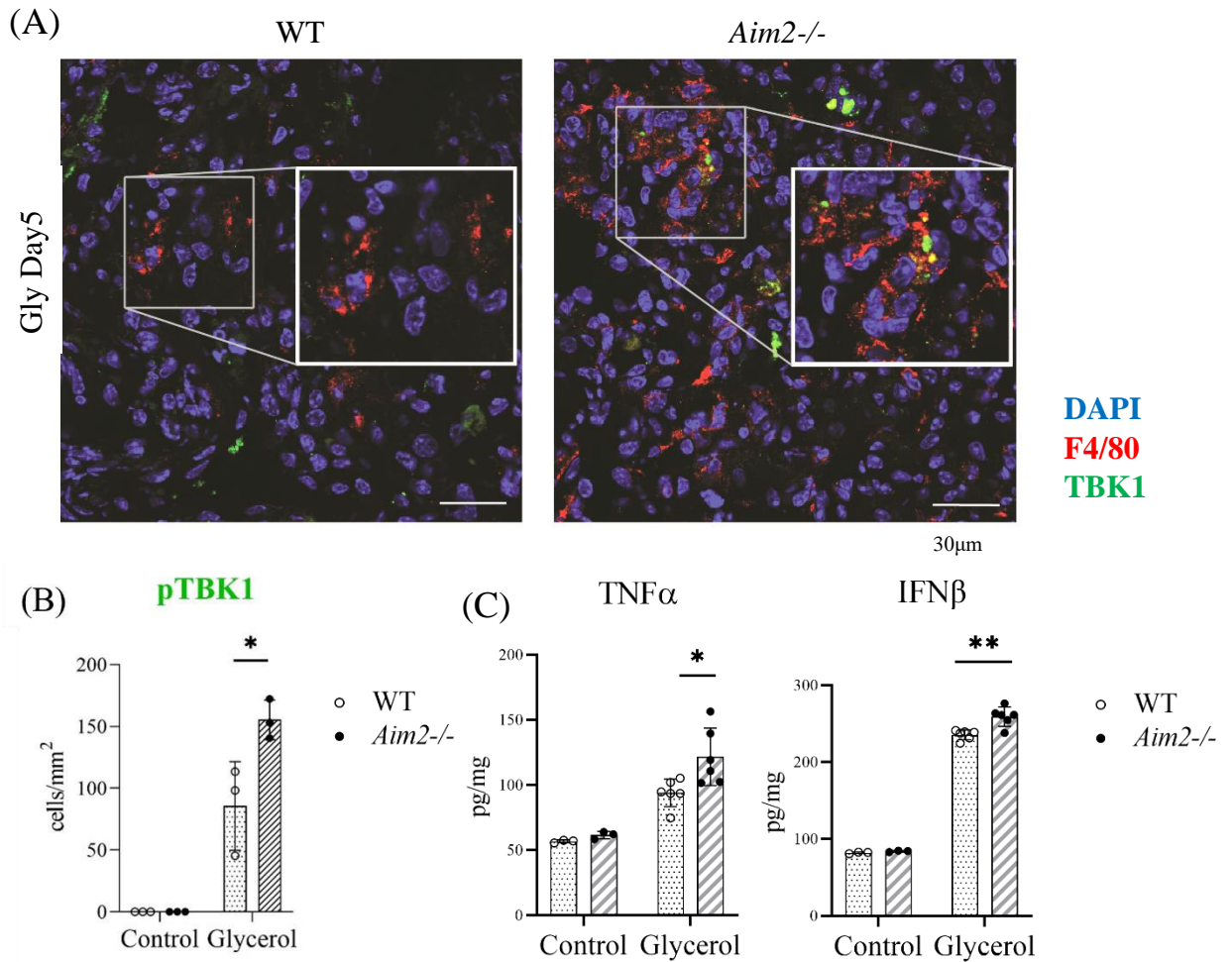


Figure 18. *Aim2*^{-/-} enhanced NF- κ B and TBK1 activation.

(A) Immunofluorescent staining for pTBK1 and F4/80 was performed on the kidney sections 5 days after RIAKI. (B) pTBK1⁺F4/80⁺ cells were quantified (n = 3 for each). (C) Total protein lysates were prepared from the kidney 5 days after glycerol treatment using RIPA lysis buffer with protease inhibitors. Kidney TNF α and IFN β were measured using ELISA. mean \pm SD; *p < 0.05 and **p < 0.01.

These results suggest that excessive fibrosis and persistent inflammation with macrophage infiltration may be caused by abnormal TBK1 activation in *Aim2*^{-/-} macrophages that escaped from pyroptosis.

3-7. dsDNA induced pyroptosis in distinct types of macrophages

In general, pyroptosis is an inflammatory type of cell death associated with secretion of mature IL-1 β /IL-18 and inhibition of inflammasome components that are beneficial in certain diseases. Surprisingly, our *in vivo* data suggest the controversial findings that deletion of *Aim2* resulted in severe fibrosis, delayed pyroptosis, increased inflammation and macrophage accumulation during RIAKI. One possible explanation for this state of *Aim2*^{-/-} mice during RIAKI is collateral activation of other inflammatory pathways, because dsDNA targets not only the AIM2 inflammasome but also other dsDNA sensors including the cGAS/STING/TBK1 pathway.

To investigate this possibility, we treated mouse mBMDM and mKRM with synthetic dsDNA (Poly (dA:dT)). In live cell imaging, membrane-impermeable dye (SYTOX red) in the cytosol of mBMDM from WT mice suggested the formation of pores on the plasma membrane, which is the characteristic phenotype of pyroptosis. In contrast, mBMDMs from *Aim2*^{-/-} mice stabilized membrane permeability for a longer time after dsDNA treatment, and the phenotype of cell death that occurred later point appeared to be different from that of WT mBMDMs (Fig. 19A).

In response to dsDNA, cell death occurred in mBMDMs from WT and *Aim2*^{-/-}, but WT mBMDMs responded more rapidly and more susceptible than *Aim2*^{-/-} mBMDMs (Fig. 19B). N-terminal GSDMD was not detected in *Aim2*^{-/-}, *Asc*^{-/-}, *Casp-1/11*^{-/-} and *Gsdmd*^{-/-} mBMDMs, and Casp-1 activation is abrogated in *Aim2*^{-/-} mBMDMs as well as *Asc*^{-/-} and *Casp1/11*^{-/-} mBMDMs. N-terminal GSDMD and active Casp-1 were detected in only WT mBMDMs after dsDNA exposure. (Fig. 19C).

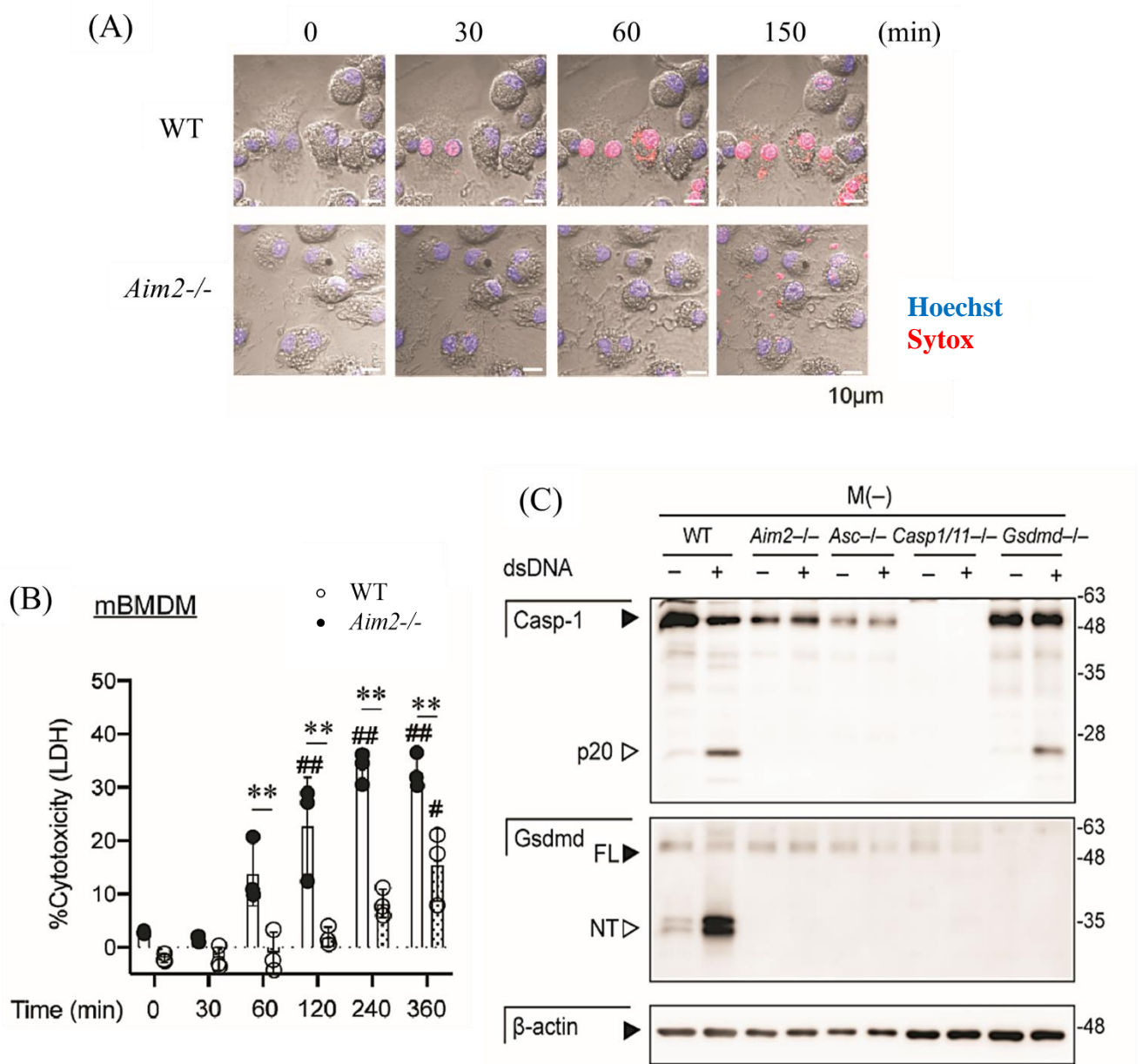


Figure 19. *Aim2*^{-/-} macrophages resistant to dsDNA-induced pyroptosis.

(A) mBMDMs derived from WT and *Aim2*^{-/-} mice were observed for 2.5 hours under time-lapse live cell imaging. Nuclei were stained with Hoechst 33342 (blue), and the cell-impermeable dye Sytox (red) detected dead nuclei. After cells were treated with dsDNA, images were taken every 10 min and are shown as bright-field, Hoechst, and Sytox overlays. (B) Cytotoxicity of dsDNA was assessed by LDH release in the supernatant (n = 3 for each group, mean ± SD; **p < 0.01. #p < 0.05 and ##p < 0.01 vs. controls at time zero). (C) Unpolarized mBMDMs (M(-)) were isolated from WT, *Aim2*^{-/-}, *Asc*^{-/-}, *Casp1/11*^{-/-}, and *Gsdmd*^{-/-} mice. Immunoblotting for caspase-1, Gsdmd, and β-actin was checked 6 hours after dsDNA treatment in a total cell/supernatant mixture.

We also isolated mKRM from WT and *Aim2*^{-/-} mice using CD11b beads and treated them with dsDNA (Fig. 20).

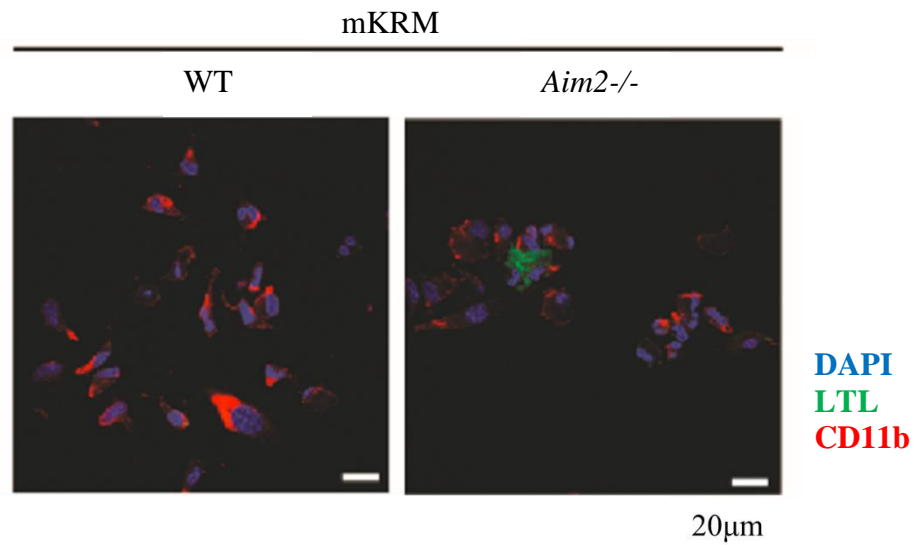


Figure 20. Kidney resident macrophage isolation. Immunofluorescent image of isolated kidney resident macrophages using CD11b magnetic beads. CD11b (red) and *Lotus tetragonolobus lectin* (LTL, a proximal tubular epithelial cell marker; green) and Hoechst 33342 (blue) was performed on isolated mKRMs and showed scarce contamination of kidney cells in isolated mKRMs.

Similar to WT mBMDMs, WT mKRMs appeared to undergo pyroptotic cell death, whereas *Aim2*^{-/-} mKRMs exhibited intact cell morphology after dsDNA treatment (Fig. 21A). Interestingly, WT mKRMs were able to produce active Casp-1 and N-terminal GSDMD, but they did not produce mature IL-1 β after dsDNA treatment. On the other hand, active Casp-1, N-terminal GSDMD, and IL-1 β were undetectable in *Aim2*^{-/-} mKRMs after dsDNA treatment (Fig. 21B, C). IL-1 β production was not detected in mKRMs by dsDNA, regardless of the presence of AIM2.

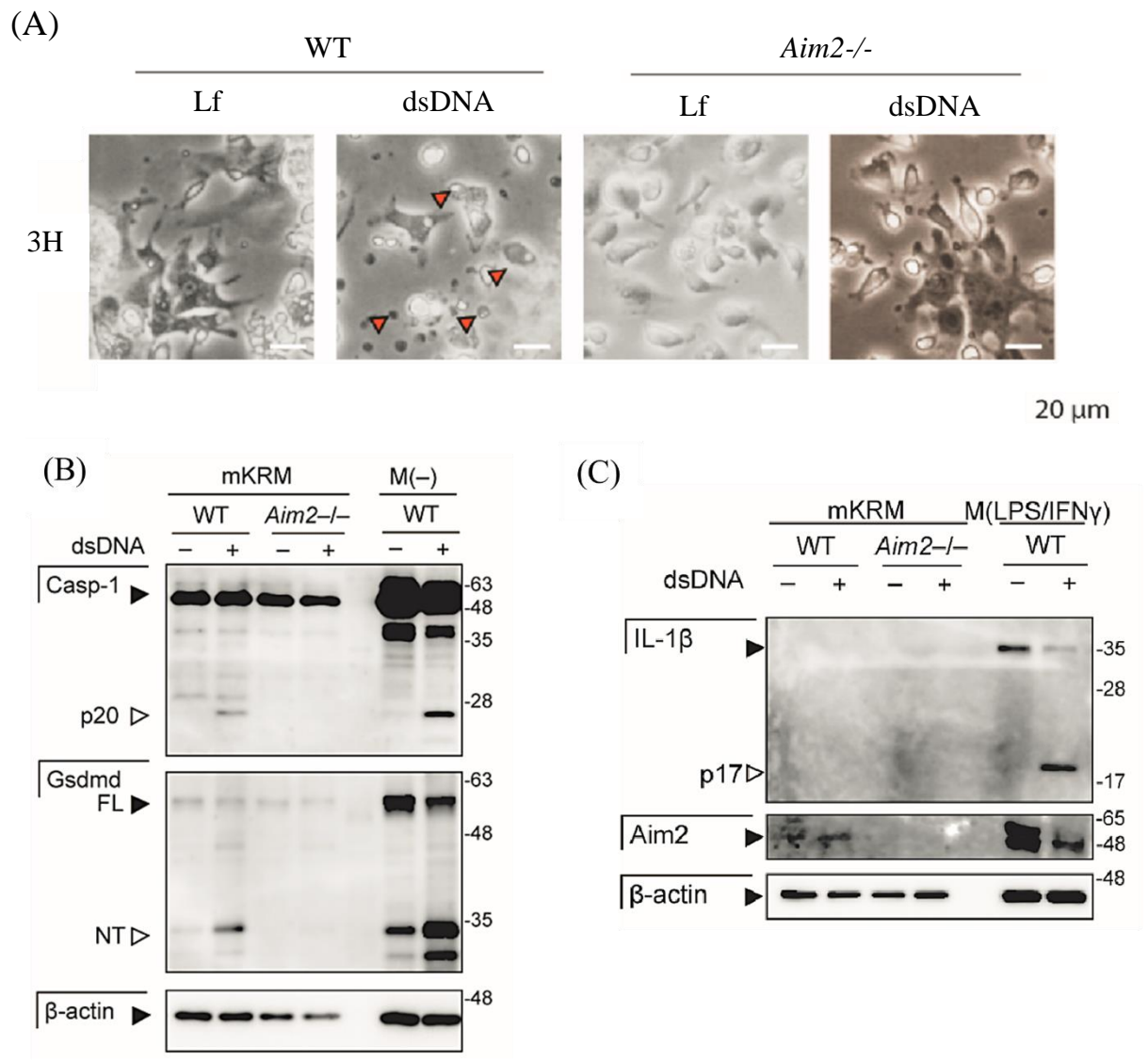


Figure 21. Kidney resident macrophages initiate dsDNA-induced pyroptosis without IL-1β release.

(A) Morphology of mKRM 3 hours after Lipofectamine (Lf) treatment with or without dsDNA. Arrows indicate dead mKRM. (B) Immunoblotting of mKRM for caspase-1, Gsdmd, and β-actin was performed 6 hours after dsDNA treatment. (C) Immunoblotting of mKRM for IL-1β, AIM2, and β-actin.

Next, we investigated the dsDNA response of different macrophage subtypes because our *in vivo* data showed M2 macrophages were dominant during RIAKI.

For this reason, we polarized WT mBMDMs into several macrophage subtypes: undifferentiated M0 macrophages without priming, M(-); M1 macrophages with LPS and IFNγ priming, M(LPS/IFNγ); M2 macrophages with IL-4 or TGFβ priming,

M(IL-4) or M(TGF β), respectively. dsDNA treatment provoked cell death (Fig. 22A) and produced the active form of Casp-1, N-terminal GSDMD not only in M(LPS/IFN γ) macrophages but also in M(-) or M(IL-4)/M(TGF β). It should be noted that pro-IL-1 β and mature IL-1 β were found in M(LPS/IFN γ) macrophages, but not in WT mBMDMs M(-) and M(IL-4)/M(TGF β) macrophages after dsDNA by western blot (Fig. 22B).

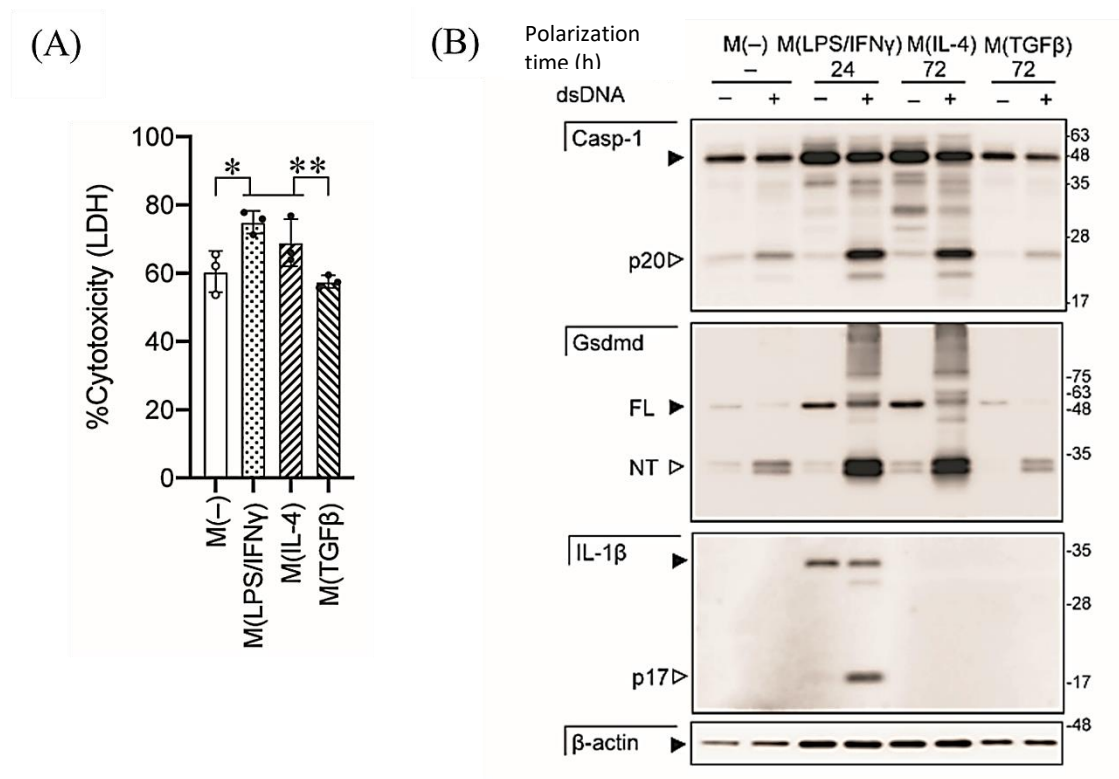


Figure 22. dsDNA induces pyroptosis in distinct types of macrophages. (A) LDH cytotoxicity assay on mBMDMs after polarization: M(-), unpolarized; M(LPS/IFN γ), M(IL-4), M(TGF β), (n = 3 for each; mean \pm SD; *p < 0.05 and **p < 0.01). (B) Immunoblotting of polarized mBMDMs for caspase-1, Gsdmd, IL-1 β , and β -actin was performed 6 hours after dsDNA treatment.

These results suggest that macrophages from WT mice are able to activate the inflammasome in response to dsDNA, regardless of their origin (recruited or resident) or polarization. These results also indicate that the outcome of AIM2-dependent inflammasome activation may differ among WT macrophages. Some WT

macrophages (mKRM, M0 and M2 mBMDMs) may undergo pyroptosis without releasing the inflammatory cytokine IL-1 β .

3-8. STING signaling enhanced inflammation by dsDNA in the *Aim2*^{-/-} macrophages.

When AIM2 is ablated, other DNA sensors are reportedly activated by dsDNA, notably cGAS. This dsDNA sensor uses the signaling pathway called STING and its downstream components TBK1 and IRF3, leading to inflammatory cytokine production. To investigate the activation of STING, we assessed the protein levels of STING, and the phosphorylated forms of TBK1, IRF3, and NF- κ B (p65) in mBMDMs from WT and *Aim2*^{-/-} after dsDNA treatment by western blot. After dsDNA treatment, mBMDMs showed activation of STING (band shift), and phosphorylation of TBK1, IRF3 and NF- κ B, regardless of polarization status in WT macrophages. However, it is found that higher levels of TBK1, IRF3 and NF- κ B were expressed in *Aim2*^{-/-} macrophages than those in WT macrophages (Fig. 23A-C). On the other hand, mTECs from *Aim2*^{-/-} mice responded similarly to dsDNA as WT mTECs. STING activation, pTBK1, pIRF3 and p-p65 were found after dsDNA transfection, but the expression levels were similar between WT and *Aim2*^{-/-} mTECs (Fig. 23D). Furthermore, immunofluorescent staining showed more phosphorylation of TBK1 in cytoplasm of *Aim2*^{-/-} macrophages compared to that of WT macrophages. (Fig. 23E, F)

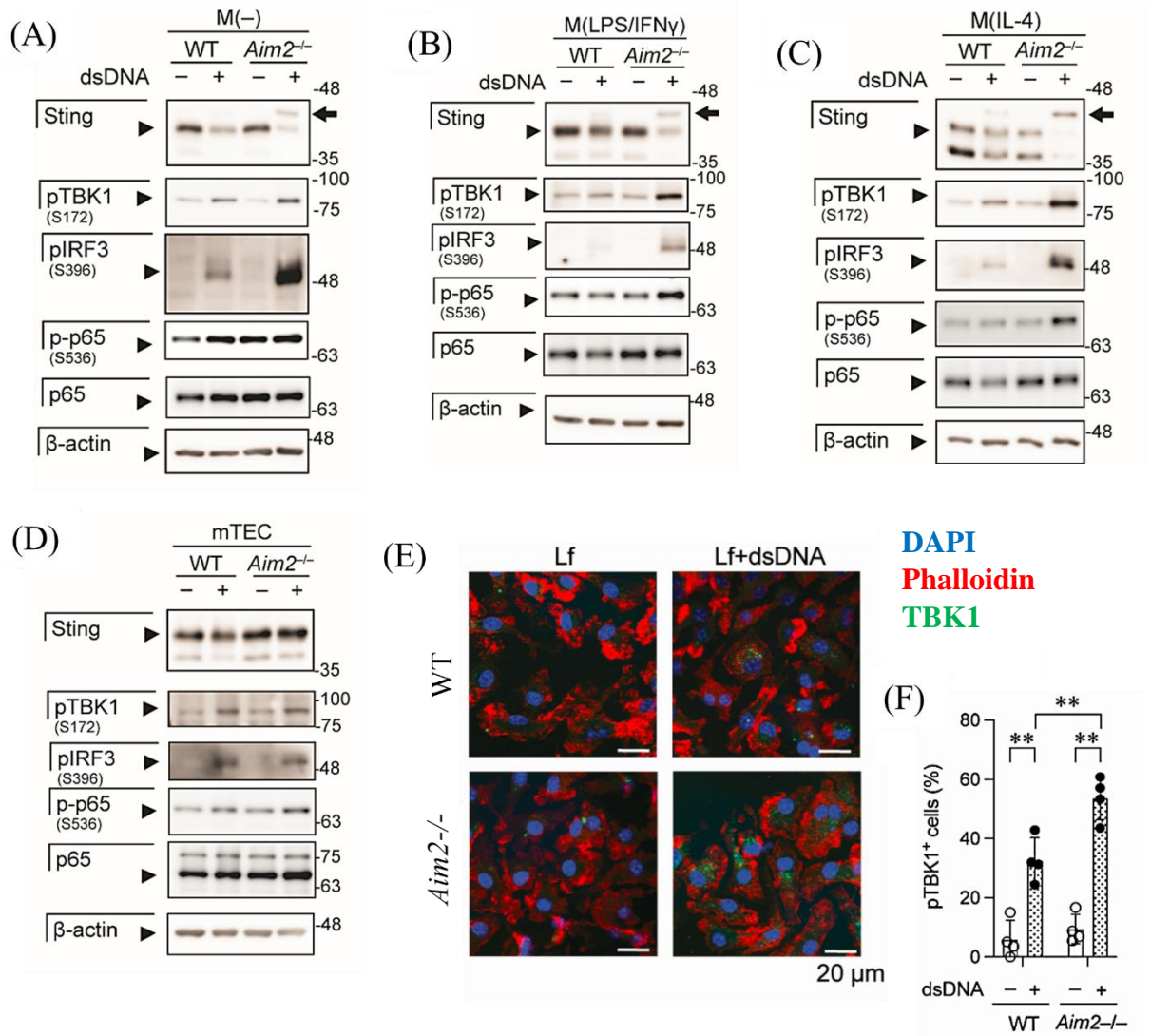


Figure 23. *Aim2*^{-/-} drives STING signaling by sensing dsDNA. (A–D) Immunoblotting analysis of Sting, phosphorylated TBK1 (Serine 172), phosphorylated IRF3 (Serine 396), p-p65 (Serine 536), total p65, and β -actin was performed on M(-) (A), M(LPS/IFN γ) (B), M(IL-4) (C), and mouse mTEC (D). Arrows indicate shifted bands of STING. (E) Immunofluorescent staining of phosphorylated TBK1 (pTBK1;green). Representative images shown. DAPI (Blue) and Phalloidin (Red) were reacted for staining nuclei and F-actin, respectively. (F) pTBK1⁺ cells were quantified (n = 4 for each; mean \pm SD; **p < 0.01).

The mRNA levels of *Cxcl10*, *Tnfa* and *Ifnb*, were upregulated more in *Aim2*^{-/-} mBMDMs than those in WT mBMDMs after dsDNA (Fig. 24A). Additionally, TNF α , and IFN β released in the medium of *Aim2*^{-/-} mBMDM detected more than those of WT mBMDM. (Fig. 24B)

Notably, release of TNF α and IFN β was suppressed by cycloheximide (CHX) and H151, indicating that cytokine overproduction in *Aim2*^{-/-} macrophages was conducted by STING-TBK1-IRF3/NF- κ B signaling under exposure to dsDNA (Fig. 24C, D).

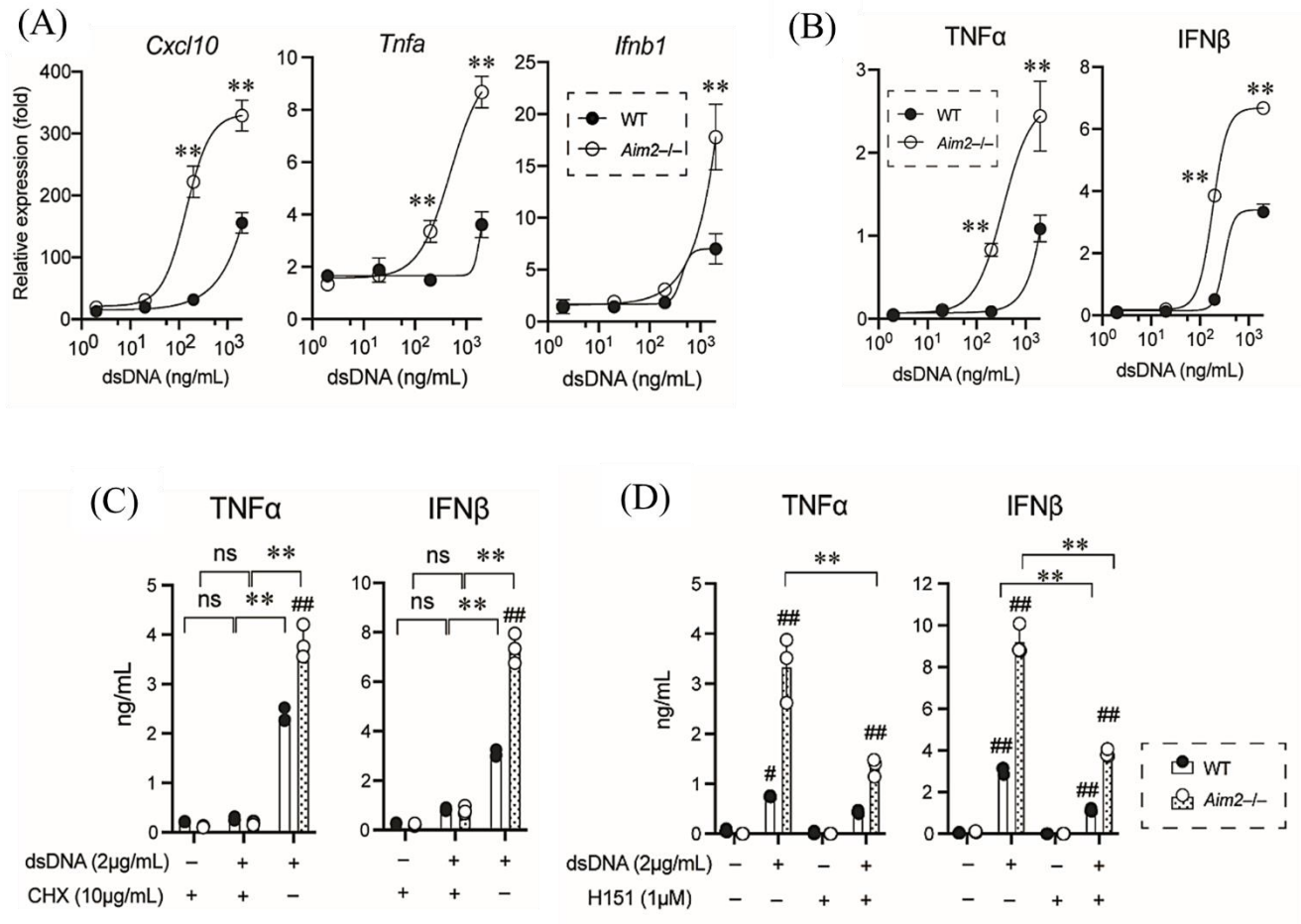


Figure 24. *Aim2*^{-/-} macrophages produced inflammatory cytokines by STING. (A) The mRNA levels of *Cxcl10*, *Tnfa*, and *Ifnb1* were analysed by real-time RT-PCR. (B) Cytokine release in the supernatant was analysed by ELISA (n = 3 for each; mean \pm SD; *p < 0.05 and **p < 0.01 vs. WT). (C) M(-) were treated with dsDNA with or without 10 μ g/mL cycloheximide (CHX). Cytokine release was analysed (n = 3 for each; mean \pm SD; *p < 0.05 and **p < 0.01. ##p < 0.01 vs. WT). (D) M(-) were treated with dsDNA with or without H151. Cytokine release was analysed (n = 3 for each; mean \pm SD; **p < 0.01. #p < 0.05 and ##p < 0.01 vs. WT)

3-9. Survived macrophages from AIM2-pyroptosis enhanced the inflammation on surrounding cells.

Finally, we assessed the effect of *Aim2*^{-/-} macrophages on surrounding cells after dsDNA exposure. To elucidate this, we collected conditioned medium (Cond. Med) from mBMDMs after dsDNA treatment. The control medium (Med) contained the same dose of dsDNA-lipofectamine complex as the conditioned medium but was incubated in a cell-free dish. Then, the Cond. Med or Med was added to murine macrophages (J774 cells) (Fig. 25A). When incubation with the Cond.Med of *Aim2*^{-/-} mBMDMs, the J774 macrophages upregulated more *Tnfa*, *Ccl2*, and *Il1b* genes than J774 macrophages incubated with Cond.Med of WT mBMDMs (Fig. 25B).

These results suggest that dsDNA does not induce inflammatory response in J774 cells, but Cond.Med from WT or *Aim2*^{-/-} mBMDMs can induce inflammation in J774 cells. In particular, Cond.Med from *Aim2*^{-/-} mBMDMs is highly inflammatory than other media.

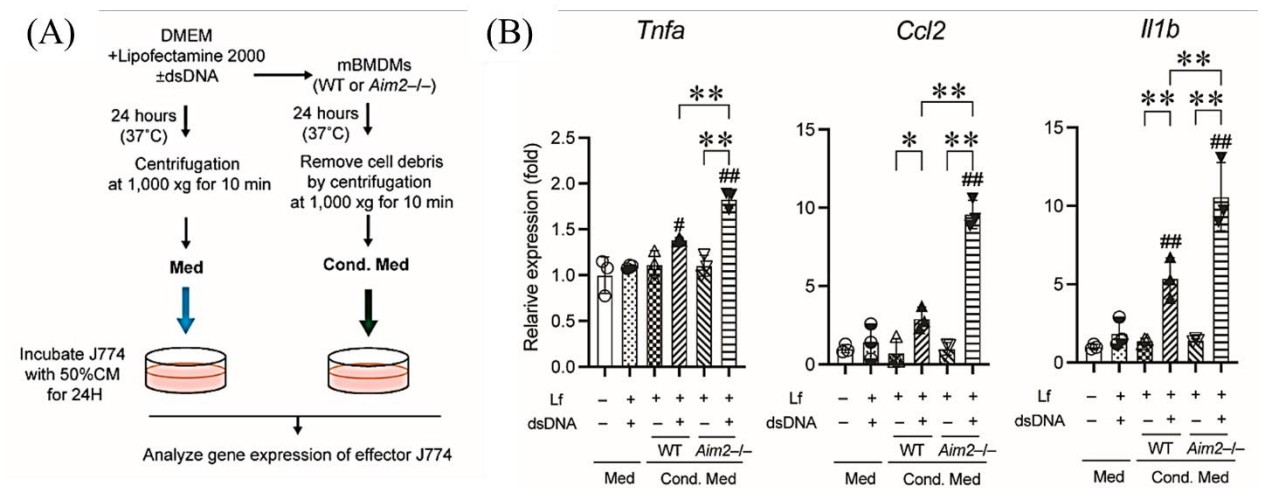


Figure 25. Escape from AIM2-pyroptosis propagates inflammation to surrounding cells. (A) The experimental design is shown. (B) The cytokine mRNA levels of effector J774 macrophages after incubation in conditioned medium (Cond. Med) were analysed by real-time RT-PCR (n = 3 for each; mean ± SD; *p < 0.05 and **p < 0.01. #p < 0.05 and ##p < 0.01 vs. controls incubated with Lf/dsDNA-free medium).

Chapter 4. Discussion

Our main findings are as follows: 1) Since DNase-I treatment improved tubular injury and inflammation, dsDNA can be a potential DAMP of RIAKI. 2) Deletion of *Aim2* resulted in prolonged injury and severe fibrosis after glycerol injection, indicating that AIM2 plays a protective role in the later stage of RIAKI. 3) CD206⁺CXCR3⁺ macrophages were the main infiltrating cells during RIAKI. 4) Pyroptosis clearly occurred in macrophages during RIAKI. 5) dsDNA induced pyroptosis without cytokine release in certain macrophages such as M0/M2 and kidney resident macrophages. In contrast, only M1 type inflammatory macrophages released cytokines after dsDNA treatment. 6) AIM2 deficiency reduced pyroptosis and delayed macrophage elimination. 7) Instead of rapid elimination by pyroptosis, *Aim2*^{-/-} macrophages activated STING to increase inflammation. 8) Humoral factors released by *Aim2*^{-/-} macrophages after dsDNA exposure prolonged the inflammatory response. These results suggest that the AIM2 inflammasome plays a protective role in RIAKI. dsDNA initiates pyroptosis in certain macrophages lacking IL-1 β production, including kidney resident and M2-polarized macrophages, but *Aim2*-deficient macrophages are resistant to dsDNA-induced pyroptosis. Survived *Aim2*^{-/-} macrophages activate STING, another type of inflammatory dsDNA sensing pathway, leading to excessive inflammation and severe fibrosis in *Aim2*^{-/-} mice after glycerol injection.

Many studies have reported that activation of the AIM2 inflammasome worsens the fate of sterile inflammatory diseases such as skin disease, diabetes, chronic kidney disease, neuronal disease, and lung diseases^{32,62-65}. In the present study, we provided new insights into the AIM2-dependent pyroptosis that limits inflammation during RIAKI.

“Homeostatic” AIM2-dependent pyroptosis in immature neurons has been recently demonstrated. Lammert, *et al.* reported that AIM2-dependent cell death contributes to the clearance of damaged neurons during brain development and showed the importance of pyroptosis for neurons during physiological condition. Similar to our study, they found that AIM2-dependent pyroptosis can be a homeostatic process to eliminate excessive cells⁶⁶.

dsDNA is a DAMP implicated in many diseases, including systemic lupus erythematosus, cancer, cystic fibrosis, diabetes, and kidney injury^{15,16,32,67-69}. During RIAKI, extracellular dsDNA exacerbates in the initial phase because our data showed that DNase-I treatment significantly improved tubular injury and inflammation. At present, it is not known which dsDNA sensor triggers inflammation in the initial phase of RIAKI. Among the various dsDNA sensors, AIM2, cGAS, DNA-PK and IFI16 are reportedly expressed in the kidney^{25,39,70}. Although, AIM2 is expressed in the tubules, podocytes, and macrophages of the kidney, and only macrophages are likely to form the AIM2 inflammasome. We showed that the activation of inflammasomes in macrophages determined by ASC speck formation in ASC-citrine mice, and the detection of N-terminal GSDMD in whole kidney lysate of WT mice after glycerol injection.

In the pathogenesis of RIAKI, dsDNA is a potential DAMP, but the origin of dsDNA is unclear. We propose possible origins of dsDNA in RIAKI. First, dsDNA can be released from necrotic cell in the kidney. Indeed, a previous study in mouse UUO model suggests that dsDNA from surrounding necrotic cells triggers AIM2-dependent pyroptosis in macrophages³². Second, dsDNA can be released from damaged muscle fibers. In this regard, we showed that plasma dsDNA increased within 1 hour after glycerol injection, suggesting that damaged muscle cells released dsDNA. However,

it is unclear how circulating dsDNA penetrates the kidney and contributes to inflammation. Third macrophage extracellular trap has been shown to be in the pathogenesis of RIAKI¹⁸. A recent study reported that the DNA network of the extracellular trap triggers AIM2-dependent pyroptosis in alveolar macrophages and contributes to the fate of acute respiratory distress syndrome (ARDS)⁶⁵. Therefore, the extracellular trap can activate the AIM2 inflammasome during RIAKI. To clarify the origin of dsDNA in RIAKI, further investigation is needed.

cGAS/STING is a dsDNA sensor expressed in most cells of the kidney. Deletion of STING alleviates inflammation and fibrosis during cisplatin-induced AKI and CKD models in mice, as activation of STING increases the production of inflammatory cytokines^{16,39}. We show that *Aim2*^{-/-} macrophages that have escaped from 'silent' pyroptosis have an extended lifespan and sufficient time to activate another dsDNA sensing pathway. Our results show that the STING inhibitor H151 is as effective as CHX in limiting cytokine release in *Aim2*^{-/-} macrophages. It is likely that rapid elimination of macrophages terminates viable cell function and limits further cytokine production. Our data demonstrate a role for AIM2-dependent pyroptosis that eliminates the macrophages rapidly before activation of the STING pathway. Consistent with our findings, previous studies have shown that activation of cGAS/STING produces type I IFNs to combat pathogens in macrophages in the absence of AIM2^{40,71}. Our *in vivo* data showed direct TBK1 activation, TNF α and IFN β production in *Aim2*^{-/-} kidney, indicating activation of STING. Furthermore, we found that CXCR3⁺ macrophage infiltration in the *Aim2*^{-/-} RIAKI kidney is likely regulated by the STING/CXCL10/CXCR3 axis. Our *in vitro* data clearly demonstrated the activation of STING in *Aim2*^{-/-} macrophages after dsDNA stimulation.

In addition, there are several reports regarding the inhibitory effect of the AIM2 inflammasome on the cGAS/ STING pathway. 1) ASC interacts with STING and inhibits TBK1 activation⁷¹. 2) Caspase-1 cleaves cGAS and arrests STING-dependent processes⁷². 3) K⁺ efflux through GSDMD pores restricted cGAS/ STING signaling⁴¹.

Also, the inhibitory effect of AIM2 on DNA-PK is reported to be independent of the inflammasome. AIM2 directly binds to DNA-PK and interrupts DNA-PK/AKT3/IRF3 signaling in microglia and reduces neuroinflammation⁴³. More studies are needed to determine how these dsDNA sensors work together to maintain homeostasis under physiological or pathological conditions.

In our study, we found massive M2 macrophage accumulation in the kidney of *Aim2*^{-/-} mice after glycerol injection. To investigating the cause of M2 macrophage accumulation, we performed cell proliferation assay because AIM2 is reported to have its inflammasome-independent role in cell proliferation, especially the tumor suppressive effect in gastric, head and neck, colorectal and other cancers^{61,73,74}. To verify the effect of AIM2 on cell proliferation during RIAKI, we performed BrdU assay in WT and *Aim2*^{-/-} mice after glycerol injection and found that cell proliferation was not altered by *Aim2* deletion. Moreover, we found upregulation of several chemokines and inflammatory cytokines *Tnfa*, *Ifnb* and *Cxcl10* in both WT and *Aim2*^{-/-} macrophages after dsDNA. As we mentioned before, *de novo* cytokine production is crucial for the pathogenesis of RIAKI according to results of CHX inhibition of those cytokines. Based on these findings, macrophage accumulation is possibly related to infiltration of circulating monocytes.

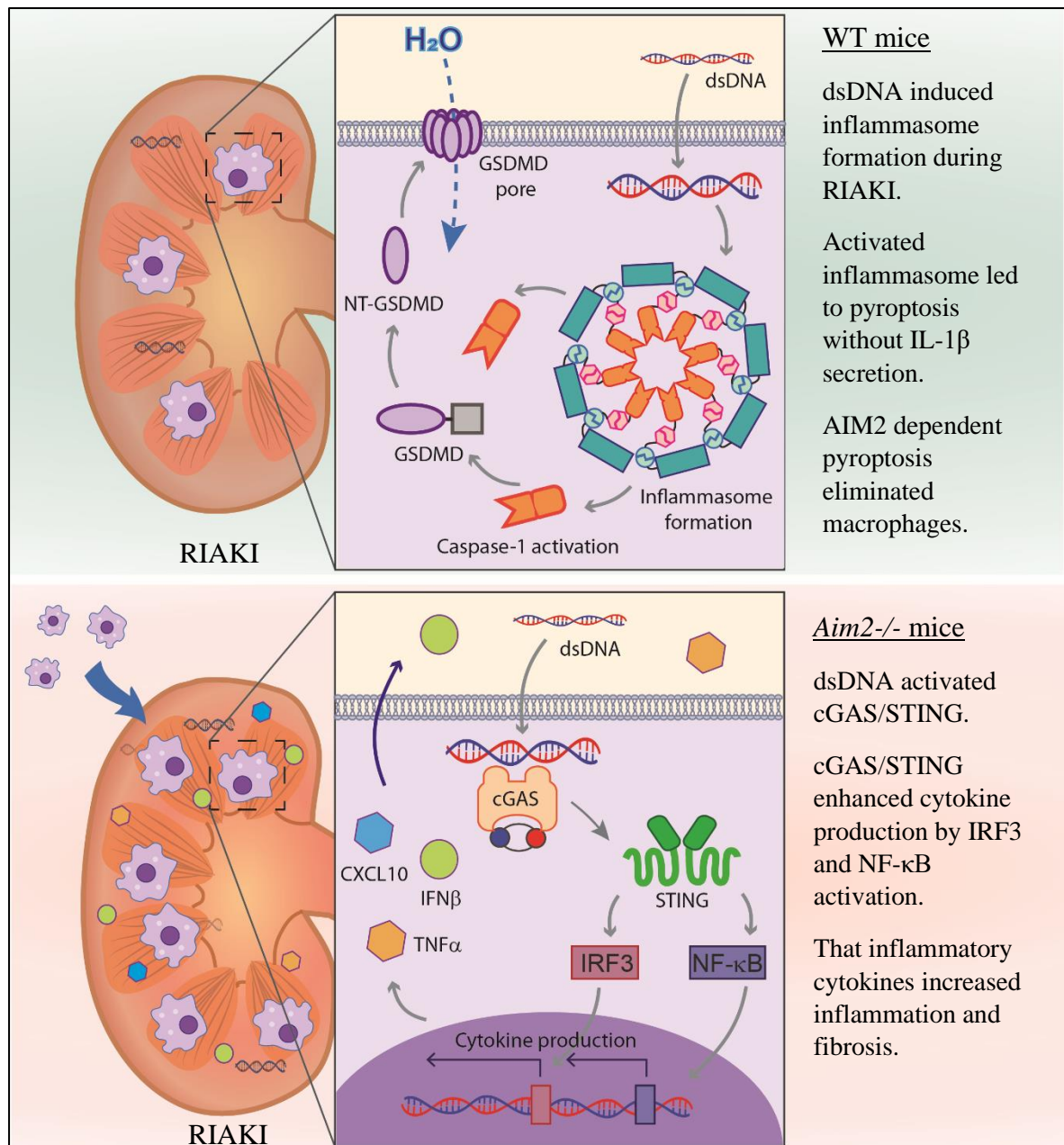


Figure 26. Graphical abstract.

(A) During the RIAKI, AIM2 dependent pyroptosis initiated by dsDNA to eliminate accumulated macrophages without cytokine production. (B) *Aim2*^{-/-} macrophages prolonged lifespan and activated cGAS/STING pathway that enhances inflammation by de novo cytokine production.

Chapter 5. Conclusion

In summary, we have demonstrated an unexpected role for AIM2-dependent pyroptosis in restricting inflammation. Previously, macrophage pyroptosis was generally considered highly inflammatory and harmful in sterile inflammatory diseases. In contrast, our findings revealed that dsDNA/AIM2-dependent “homeostatic” pyroptosis in macrophages is essential for normal healing during RIAKI.

References

1. Warren JD, Blumbergs PC, Thompson PD. Rhabdomyolysis: a review. *Muscle Nerve*. 25(3):332-347,2002.
2. Gabow PA, Kaehny WD, Kelleher SP. The spectrum of rhabdomyolysis. *Medicine (Baltimore)*. 61(3):141-152,1982.
3. Harriston S. A review of rhabdomyolysis. *Dimens Crit Care Nurs*. 23(4):155-161,2004.
4. Marc L Miller. Causes. In: Ira N Targoff JMS, John F Dashe, ed. *Causes of rhabdomyolysis*. uptodate.com2021.
5. Chatzizisis YS, Misirli G, Hatzitolios AI, Giannoglou GD. The syndrome of rhabdomyolysis: complications and treatment. *Eur J Intern Med*. 19(8):568-574,2008.
6. Stanley M, Chippa V, Aeddula NR, Quintanilla Rodriguez BS, Adigun R. Rhabdomyolysis. *StatPearls*. Treasure Island (FL)2021.
7. Huerta-Alardin AL, Varon J, Marik PE. Bench-to-bedside review: Rhabdomyolysis -- an overview for clinicians. *Crit Care*. 9(2):158-169,2005.
8. Kasaoka S, Todani M, Kaneko T, Kawamura Y, Oda Y, Tsuruta R, Maekawa T. Peak value of blood myoglobin predicts acute renal failure induced by rhabdomyolysis. *J Crit Care*. 25(4):601-604,2010.
9. Melli G, Chaudhry V, Cornblath DR. Rhabdomyolysis: an evaluation of 475 hospitalized patients. *Medicine (Baltimore)*. 84(6):377-385,2005.
10. McMahon GM, Zeng X, Waikar SS. A risk prediction score for kidney failure or mortality in rhabdomyolysis. *JAMA Intern Med*. 173(19):1821-1828,2013.
11. Candela N, Silva S, Georges B, Cartery C, Robert T, Moussi-Frances J, Rondeau E, Rebibou JM, Lavayssiere L, Belliere J, Krummel T, Lebas C, Cointault O, Sallee M, Faguer S, French Intensive Care Renal N. Short- and long-term renal outcomes following severe rhabdomyolysis: a French multicenter retrospective study of 387 patients. *Ann Intensive Care*. 10(1):27,2020.
12. Bosch X, Poch E, Grau JM. Rhabdomyolysis and acute kidney injury. *N Engl J Med*. 361(1):62-72,2009.
13. Bai Y, Tong Y, Liu Y, Hu H. Self-dsDNA in the pathogenesis of systemic lupus erythematosus. *Clin Exp Immunol*. 191(1):1-10,2018.

14. Njeim R, Azar WS, Fares AH, Azar ST, Kfoury Kassouf H, Eid AA. NETosis contributes to the pathogenesis of diabetes and its complications. *J Mol Endocrinol.* 65(4):R65-R76,2020.
15. Benmerzoug S, Rose S, Bounab B, Gosset D, Duneau L, Chenuet P, Mollet L, Le Bert M, Lambers C, Geleff S, Roth M, Fauconnier L, Sedda D, Carvalho C, Perche O, Laurenceau D, Ryffel B, Apetoh L, Kiziltunc A, Uslu H, Albez FS, Akgun M, Togbe D, Quesniaux VFJ. STING-dependent sensing of self-DNA drives silica-induced lung inflammation. *Nat Commun.* 9(1):5226,2018.
16. Maekawa H, Inoue T, Ouchi H, Jao TM, Inoue R, Nishi H, Fujii R, Ishidate F, Tanaka T, Tanaka Y, Hirokawa N, Nangaku M, Inagi R. Mitochondrial Damage Causes Inflammation via cGAS-STING Signaling in Acute Kidney Injury. *Cell Rep.* 29(5):1261-1273 e1266,2019.
17. Liu J, Jia Z, Gong W. Circulating Mitochondrial DNA Stimulates Innate Immune Signaling Pathways to Mediate Acute Kidney Injury. *Front Immunol.* 12:680648,2021.
18. Okubo K, Kurosawa M, Kamiya M, Urano Y, Suzuki A, Yamamoto K, Hase K, Homma K, Sasaki J, Miyauchi H, Hoshino T, Hayashi M, Mayadas TN, Hirahashi J. Macrophage extracellular trap formation promoted by platelet activation is a key mediator of rhabdomyolysis-induced acute kidney injury. *Nat Med.* 24(2):232-238,2018.
19. DeYoung KL, Ray ME, Su YA, Anzick SL, Johnstone RW, Trapani JA, Meltzer PS, Trent JM. Cloning a novel member of the human interferon-inducible gene family associated with control of tumorigenicity in a model of human melanoma. *Oncogene.* 15(4):453-457,1997.
20. Bürckstümmer T, Baumann C., Blüml S. et al. An orthogonal proteomic-genomic screen identifies AIM2 as a cytoplasmic DNA sensor for the inflammasome. *Nat Immunol.* 10:266-272,2009.
21. Fernandes-Alnemri T, Yu JW, Datta P, Wu J, Alnemri ES. AIM2 activates the inflammasome and cell death in response to cytoplasmic DNA. *Nature.* 458(7237):509-513,2009.
22. Hornung V, Ablasser A, Charrel-Dennis M, Bauernfeind F, Horvath G, Caffrey DR, Latz E, Fitzgerald KA. AIM2 recognizes cytosolic dsDNA and forms a caspase-1-activating inflammasome with ASC. *Nature.* 458(7237):514-518,2009.

23. Roberts TL, Idris A, Dunn JA, Kelly GM, Burnton CM, Hodgson S, Hardy LL, Garceau V, Sweet MJ, Ross IL, Hume DA, Stacey KJ. HIN-200 proteins regulate caspase activation in response to foreign cytoplasmic DNA. *Science*. 323(5917):1057-1060,2009.
24. Lugrin J, Martinon F. The AIM2 inflammasome: Sensor of pathogens and cellular perturbations. *Immunol Rev*. 281(1):99-114,2018.
25. Komada T, Muruve DA. The role of inflammasomes in kidney disease. *Nat Rev Nephrol*. 15(8):501-520,2019.
26. Kim SM, Kim YG, Kim DJ, Park SH, Jeong KH, Lee YH, Lim SJ, Lee SH, Moon JY. Inflammasome-Independent Role of NLRP3 Mediates Mitochondrial Regulation in Renal Injury. *Front Immunol*. 9:2563,2018.
27. Elsayed MS, Abu-Elsaad NM, Nader MA. The NLRP3 inhibitor dapansutrile attenuates folic acid induced nephrotoxicity via inhibiting inflammasome/caspase-1/IL axis and regulating autophagy/proliferation. *Life Sci*. 285:119974,2021.
28. Li S, Lin Q, Shao X, Mou S, Gu L, Wang L, Zhang Z, Shen J, Zhou Y, Qi C, Jin H, Pang H, Ni Z. NLRP3 inflammasome inhibition attenuates cisplatin-induced renal fibrosis by decreasing oxidative stress and inflammation. *Exp Cell Res*. 383(1):111488,2019.
29. Sakai N, Furuichi K, Wada T. Inhibition of NLRP3 inflammasome as a therapeutic intervention in crystal-induced nephropathy. *Kidney Int*. 90(3):466-468,2016.
30. Lin Q, Li S, Jiang N, Jin H, Shao X, Zhu X, Wu J, Zhang M, Zhang Z, Shen J, Zhou W, Gu L, Lu R, Ni Z. Inhibiting NLRP3 inflammasome attenuates apoptosis in contrast-induced acute kidney injury through the upregulation of HIF1A and BNIP3-mediated mitophagy. *Autophagy*. 17(10):2975-2990,2021.
31. Komada T, Usui F, Kawashima A, Kimura H, Karasawa T, Inoue Y, Kobayashi M, Mizushima Y, Kasahara T, Taniguchi S, Muto S, Nagata D, Takahashi M. Role of NLRP3 Inflammasomes for Rhabdomyolysis-induced Acute Kidney Injury. *Sci Rep*. 5:10901,2015.
32. Komada T, Chung H, Lau A, Platnich JM, Beck PL, Benediktsson H, Duff HJ, Jenne CN, Muruve DA. Macrophage Uptake of Necrotic Cell DNA Activates the AIM2 Inflammasome to Regulate a Proinflammatory Phenotype in CKD. *J Am Soc Nephrol*. 29(4):1165-1181,2018.

33. Decout A, Katz JD, Venkatraman S, Ablasser A. The cGAS-STING pathway as a therapeutic target in inflammatory diseases. *Nat Rev Immunol.* 21(9):548-569,2021.
34. Jiang M, Chen P, Wang L, Li W, Chen B, Liu Y, Wang H, Zhao S, Ye L, He Y, Zhou C. cGAS-STING, an important pathway in cancer immunotherapy. *J Hematol Oncol.* 13(1):81,2020.
35. Thim-Uam A, Prabakaran T, Tansakul M, Makjaroen J, Wongkongkathap P, Chantaravisoot N, Saethang T, Leelahavanichkul A, Benjachat T, Paludan S, Pisitkun T, Pisitkun P. STING Mediates Lupus via the Activation of Conventional Dendritic Cell Maturation and Plasmacytoid Dendritic Cell Differentiation. *iScience.* 23(9):101530,2020.
36. Yu Y, Liu Y, An W, Song J, Zhang Y, Zhao X. STING-mediated inflammation in Kupffer cells contributes to progression of nonalcoholic steatohepatitis. *J Clin Invest.* 129(2):546-555,2019.
37. Abdullah A, Zhang M, Frugier T, Bedoui S, Taylor JM, Crack PJ. STING-mediated type-I interferons contribute to the neuroinflammatory process and detrimental effects following traumatic brain injury. *J Neuroinflammation.* 15(1):323,2018.
38. King KR, Aguirre AD, Ye YX, Sun Y, Roh JD, Ng RP, Jr., Kohler RH, Arlauckas SP, Iwamoto Y, Savol A, Sadreyev RI, Kelly M, Fitzgibbons TP, Fitzgerald KA, Mitchison T, Libby P, Nahrendorf M, Weissleder R. IRF3 and type I interferons fuel a fatal response to myocardial infarction. *Nat Med.* 23(12):1481-1487,2017.
39. Chung KW, Dhillon P, Huang S, Sheng X, Shrestha R, Qiu C, Kaufman BA, Park J, Pei L, Baur J, Palmer M, Susztak K. Mitochondrial Damage and Activation of the STING Pathway Lead to Renal Inflammation and Fibrosis. *Cell Metab.* 30(4):784-799 e785,2019.
40. Corrales L, Woo SR, Williams JB, McWhirter SM, Dubensky TW, Jr., Gajewski TF. Antagonism of the STING Pathway via Activation of the AIM2 Inflammasome by Intracellular DNA. *J Immunol.* 196(7):3191-3198,2016.
41. Banerjee I, Behl B, Mendonca M, Shrivastava G, Russo AJ, Menoret A, Ghosh A, Vella AT, Vanaja SK, Sarkar SN, Fitzgerald KA, Rathinam VAK. Gasdermin D Restrains Type I Interferon Response to Cytosolic DNA by Disrupting Ionic Homeostasis. *Immunity.* 49(3):413-426 e415,2018.

42. Wilson JE, Petrucelli AS, Chen L, Koblansky AA, Truax AD, Oyama Y, Rogers AB, Brickey WJ, Wang Y, Schneider M, Muhlbauer M, Chou WC, Barker BR, Jobin C, Allbritton NL, Ramsden DA, Davis BK, Ting JP. Inflammasome-independent role of AIM2 in suppressing colon tumorigenesis via DNA-PK and Akt. *Nat Med.* 21(8):906-913,2015.
43. Ma C, Li S, Hu Y, Ma Y, Wu Y, Wu C, Liu X, Wang B, Hu G, Zhou J, Yang S. AIM2 controls microglial inflammation to prevent experimental autoimmune encephalomyelitis. *J Exp Med.* 218(5),2021.
44. Brodsky IE, Medzhitov R. Pyroptosis: macrophage suicide exposes hidden invaders. *Curr Biol.* 21(2):R72-75,2011.
45. Vande Walle L, Lamkanfi M. Pyroptosis. *Curr Biol.* 26(13):R568-R572,2016.
46. Baek JH. The Impact of Versatile Macrophage Functions on Acute Kidney Injury and Its Outcomes. *Front Physiol.* 10:1016,2019.
47. Belliere J, Casemayou A, Ducasse L, Zakaroff-Girard A, Martins F, Iacovoni JS, Guilbeau-Frugier C, Buffin-Meyer B, Pipy B, Chauveau D, Schanstra JP, Bascands JL. Specific macrophage subtypes influence the progression of rhabdomyolysis-induced kidney injury. *J Am Soc Nephrol.* 26(6):1363-1377,2015.
48. Chen T, Cao Q, Wang Y, Harris DCH. M2 macrophages in kidney disease: biology, therapies, and perspectives. *Kidney Int.* 95(4):760-773,2019.
49. Kim MG, Kim SC, Ko YS, Lee HY, Jo SK, Cho W. The Role of M2 Macrophages in the Progression of Chronic Kidney Disease following Acute Kidney Injury. *PLoS One.* 10(12):e0143961,2015.
50. Kim MG, Lim K, Lee YJ, Yang J, Oh SW, Cho WY, Jo SK. M2 macrophages predict worse long-term outcomes in human acute tubular necrosis. *Sci Rep.* 10(1):2122,2020.
51. Mizuno-Iijima S, Ayabe S, Kato K, Matoba S, Ikeda Y, Dinh TTH, Le HT, Suzuki H, Nakashima K, Hasegawa Y, Hamada Y, Tanimoto Y, Daitoku Y, Iki N, Ishida M, Ibrahim EAE, Nakashiba T, Hamada M, Murata K, Miwa Y, Okada-Iwabuchi M, Iwabuchi M, Yagami KI, Ogura A, Obata Y, Takahashi S, Mizuno S, Yoshiki A, Sugiyama F. Efficient production of large deletion and gene fragment knock-in mice mediated by genome editing with Cas9-mouse Cdt1 in mouse zygotes. *Methods.* 191:23-31,2021.

52. Yamamoto M, Yaginuma K, Tsutsui H, Sagara J, Guan X, Seki E, Yasuda K, Yamamoto M, Akira S, Nakanishi K, Noda T, Taniguchi S. ASC is essential for LPS-induced activation of procaspase-1 independently of TLR-associated signal adaptor molecules. *Genes Cells*. 9(11):1055-1067,2004.
53. Kuida K, Lippke JA, Ku G, Harding MW, Livingston DJ, Su MS, Flavell RA. Altered cytokine export and apoptosis in mice deficient in interleukin-1 beta converting enzyme. *Science*. 267(5206):2000-2003,1995.
54. Tsutsui H, Kayagaki N, Kuida K, Nakano H, Hayashi N, Takeda K, Matsui K, Kashiwamura S, Hada T, Akira S, Yagita H, Okamura H, Nakanishi K. Caspase-1-independent, Fas/Fas ligand-mediated IL-18 secretion from macrophages causes acute liver injury in mice. *Immunity*. 11(3):359-367,1999.
55. Kayagaki N, Stowe IB, Lee BL, O'Rourke K, Anderson K, Warming S, Cuellar T, Haley B, Roose-Girma M, Phung QT, Liu PS, Lill JR, Li H, Wu J, Kummerfeld S, Zhang J, Lee WP, Snipas SJ, Salvesen GS, Morris LX, Fitzgerald L, Zhang Y, Bertram EM, Goodnow CC, Dixit VM. Caspase-11 cleaves gasdermin D for non-canonical inflammasome signalling. *Nature*. 526(7575):666-671,2015.
56. Tzeng TC, Schattgen S, Monks B, Wang D, Cerny A, Latz E, Fitzgerald K, Golenbock DT. A Fluorescent Reporter Mouse for Inflammasome Assembly Demonstrates an Important Role for Cell-Bound and Free ASC Specks during In Vivo Infection. *Cell Rep*. 16(2):571-582,2016.
57. Singh AP, Junemann A, Muthuraman A, Jaggi AS, Singh N, Grover K, Dhawan R. Animal models of acute renal failure. *Pharmacol Rep*. 64(1):31-44,2012.
58. Chawla LS, Eggers PW, Star RA, Kimmel PL. Acute kidney injury and chronic kidney disease as interconnected syndromes. *N Engl J Med*. 371(1):58-66,2014.
59. Groom JR, Luster AD. CXCR3 ligands: redundant, collaborative and antagonistic functions. *Immunol Cell Biol*. 89(2):207-215,2011.
60. Xu M, Wang J, Li H, Zhang Z, Cheng Z. AIM2 inhibits colorectal cancer cell proliferation and migration through suppression of Gli1. *Aging (Albany NY)*. 13(1):1017-1031,2020.

61. Wang D, Zou J, Dai J, Cheng Z. Absent in melanoma 2 suppresses gastric cancer cell proliferation and migration via inactivation of AKT signaling pathway. *Sci Rep.* 11(1):8235,2021.
62. Dombrowski Y, Peric M, Koglin S, Kammerbauer C, Goss C, Anz D, Simanski M, Glaser R, Harder J, Hornung V, Gallo RL, Ruzicka T, Besch R, Schaubert J. Cytosolic DNA triggers inflammasome activation in keratinocytes in psoriatic lesions. *Sci Transl Med.* 3(82):82ra38,2011.
63. Wang X, Pan J, Liu H, Zhang M, Liu D, Lu L, Tian J, Liu M, Jin T, An F. AIM2 gene silencing attenuates diabetic cardiomyopathy in type 2 diabetic rat model. *Life Sci.* 221:249-258,2019.
64. Kim H, Seo JS, Lee SY, Ha KT, Choi BT, Shin YI, Ju Yun Y, Shin HK. AIM2 inflammasome contributes to brain injury and chronic post-stroke cognitive impairment in mice. *Brain Behav Immun.* 87:765-776,2020.
65. Li H, Li Y, Song C, Hu Y, Dai M, Liu B, Pan P. Neutrophil Extracellular Traps Augmented Alveolar Macrophage Pyroptosis via AIM2 Inflammasome Activation in LPS-Induced ALI/ARDS. *J Inflamm Res.* 14:4839-4858,2021.
66. Lammert CR, Frost EL, Bellinger CE, Bolte AC, McKee CA, Hurt ME, Paysour MJ, Ennerfelt HE, Lukens JR. AIM2 inflammasome surveillance of DNA damage shapes neurodevelopment. *Nature.* 580(7805):647-652,2020.
67. Pisetsky DS. The complex role of DNA, histones and HMGB1 in the pathogenesis of SLE. *Autoimmunity.* 47(8):487-493,2014.
68. Cao Q, Xu W, Wen Z, Xu L, Li K, Chu Y, Xiong S. An anti-double-stranded DNA monoclonal antibody induced by tumor cell-derived DNA inhibits the growth of tumor in vitro and in vivo via triggering apoptosis. *DNA Cell Biol.* 27(2):91-100,2008.
69. Nie L, Zhao P, Yue Z, Zhang P, Ji N, Chen Q, Wang Q. Diabetes induces macrophage dysfunction through cytoplasmic dsDNA/AIM2 associated pyroptosis. *J Leukoc Biol.* 110(3):497-510,2021.
70. Chandra AN, Saravanabavan S, Rangan GK. Role of DNA-Dependent Protein Kinase in Mediating Cyst Growth in Autosomal Dominant Polycystic Kidney Disease. *Int J Mol Sci.* 22(19),2021.
71. Yan S, Shen H, Lian Q, Jin W, Zhang R, Lin X, Gu W, Sun X, Meng G, Tian Z, Chen ZW, Sun B. Deficiency of the AIM2-ASC Signal Uncovers the STING-Driven Overreactive Response of Type I IFN and Reciprocal

- Depression of Protective IFN-gamma Immunity in Mycobacterial Infection. *J Immunol.* 200(3):1016-1026,2018.
72. Wang Y, Ning X, Gao P, Wu S, Sha M, Lv M, Zhou X, Gao J, Fang R, Meng G, Su X, Jiang Z. Inflammasome Activation Triggers Caspase-1-Mediated Cleavage of cGAS to Regulate Responses to DNA Virus Infection. *Immunity.* 46(3):393-404,2017.
 73. Li Z, Shi X, Li H, Wang W, Li X. Low expression of AIM2 combined with high expression of pSTAT3 is associated with poor prognosis in hypopharyngeal squamous cell carcinoma. *Oncol Rep.* 41(4):2396-2408,2019.
 74. Shah S, Qin S, Luo Y, Huang Y, Jing R, Shah JN, Chen J, Chen H, Zhong M. AIM2 Inhibits BRAF-Mutant Colorectal Cancer Growth in a Caspase-1-Dependent Manner. *Front Cell Dev Biol.* 9:588278,2021.